5-18-93
E-7566

NASA Technical Memorandum 105987

Low Cycle Fatigue Behavior of Polycrystalline NiAl at 300 and 1000 K

Bradley A. Lerch and Ronald D. Noebe
Lewis Research Center
Cleveland, Ohio

April 1993

NASA

LOW CYCLE FATIGUE BEHAVIOR OF POLYCRYSTALLINE NiAl AT 300 AND 1000 K

Bradley A. Lerch and Ronald D. Noebe
NASA Lewis Research Center
Cleveland, Ohio 44135

SUMMARY

The low cycle fatigue behavior of polycrystalline NiAl was determined at 300 and 1000 K—temperatures below and above the brittle-to-ductile transition temperature (BDTT). Fully reversed, plastic strain-controlled fatigue tests were conducted on two differently fabricated alloy samples: hot isostatically pressed (HIP'ed) prealloyed powder and hot extruded castings. HIP'ed powder (HP) samples were tested only at 1000 K, whereas the more ductile cast-and-extruded (C+E) NiAl samples were tested at both 1000 and 300 K. Plastic strain ranges of 0.06 to 0.2 percent were used. The C+E NiAl cyclically hardened until fracture, reaching stress levels approximately 60 percent greater than the ultimate tensile strength of the alloy. Compared on a strain basis, NiAl had a much longer fatigue life than other B2 ordered compounds in which fracture initiated at processing-related defects. These defects controlled fatigue life at 300 K, with fracture occurring rapidly once a critical stress level was reached.

At 1000 K, above the BDTT, both the C+E and HP samples cyclically softened during most of the fatigue tests in air and were insensitive to processing defects. The processing method did not have a major effect on fatigue life; the lives of the HP samples were about a factor of three shorter than the C+E NiAl, but this was attributed to the lower stress response of the C+E material. The C+E NiAl underwent dynamic grain growth, whereas the HP material maintained a constant grain size during testing. In both materials, fatigue life was controlled by intergranular cavitation and creep processes, which led to fatigue crack growth that was primarily intergranular in nature. Final fracture by overload was transgranular in nature. Also, HP samples tested in vacuum had a life three times longer than their counterparts tested in air and, in contrast to those tested in air, hardened continuously over half of the sample life, thereby indicating an environmentally assisted fatigue damage mechanism. The C+E samples were tested only in air. At 1000 K, NiAl exhibited a superior fatigue life when compared to most superalloys on a plastic strain basis, but was inferior to most superalloys on a stress basis.

INTRODUCTION

There is considerable interest in developing new structural materials that, at a minimum, have high use temperatures, and strength coupled with low density. The desire is to go well beyond the working range of strengths and temperatures provided by superalloys. In response to this need, ordered intermetallic alloys have been the subject of extensive investigation. Of the many intermetallic alloys under consideration, NiAl is one of the few systems that has emerged as a promising candidate for further development. This is due to a number of property advantages, including low density, high melting point, high thermal conductivity, excellent environmental resistance, and the potential for significantly improving creep resistance through alloying (refs. 1 and 2). However, minimal ductility at lower temperatures remains a limitation of NiAl.

Prior to 1989 only one study (ref. 3) had reported measurable room temperature tensile ductility for the B2 intermetallic compound NiAl. This lack of tensile ductility is due to an insufficient number of

independent slip systems to accommodate general polycrystalline deformation (ref. 4) and has precluded any serious attempt at investigating advanced properties such as fatigue. Instead, recent emphasis has been on increasing the ductility of polycrystalline NiAl through alloying (refs. 5 to 7) and improved processing techniques (refs. 7 to 11). Although improving ductility through alloying has been unsuccessful to date, efforts at improving the processing and cleanliness of stoichiometric binary NiAl have resulted in limited, but at least consistent and reproducible, room temperature ductility on the order of 1 to 3 percent (refs. 6 to 11).

At intermediate temperatures, tensile ductility is no longer a use-limiting property since extruded binary NiAl undergoes a brittle-to-ductile transition between approximately 550 and 700 K, with dramatic increases in tensile elongation (refs. 2, 3, 5, 6, and 10 to 12) and fracture strength and toughness (refs. 13 and 14) occurring in this temperature range. Although the mechanism responsible for this change in behavior is not fully resolved, it is generally agreed (refs. 2 and 12) that the brittle-to-ductile transition temperature (BDTT) is a result of diffusion-assisted deformation processes, as first proposed by Ball and Smallman (ref. 15). At temperatures above the BDTT the majority of investigations have focused on the compressive creep behavior of binary NiAl (refs. 16 and 17) and NiAl-based composites (ref. 18).

Through these efforts (refs. 1 to 18) a reasonable understanding of the monotonic behavior of NiAl has been achieved. However, little information is available on the cyclic flow and fracture behavior of NiAl. Such information is necessary to determine whether fatigue is a limiting property for this potential structural material. Understanding cyclic properties may also provide insight into the behavior of the NiAl matrix phase in thermally cycled composites where strains develop through thermal expansion mismatch between the matrix and fiber. Identification of the mechanisms controlling fatigue life at both low and high temperatures will also guide second generation alloy development and processing efforts.

Several efforts are presently underway to investigate various aspects of NiAl fatigue behavior. Preliminary testing in both strain and load control of single crystal NiAl has been performed on a <001> single crystal Ni-49.9Al-0.1Mo alloy by K.W. Bain et al. (G.E. Aircraft Engines, Evandale, OH; unpublished paper, "Fatigue Behavior of NiAl Single Crystals," presented at the fall TMS meeting, 1991). Data for this alloy were generated primarily at 1033 K, with room temperature tests exhibiting only elastic behavior before failure. At 1033 K, the single crystals exhibited a Coffin-Manson strain life behavior, with fatigue lives that were greater than René N4 at high strain ranges, which was attributed to the greater ductility of the NiAl. Failure of these samples was unusual: cracks occurred parallel to the axis of loading. Bowman (ref. 19) performed room temperature fatigue tests on NiAl and NiAl/Al_2O_3 composites under displacement control between set stress ranges. He determined that for up to 100 000 cycles the presence of the fibers did not degrade the fatigue properties of the NiAl as long as the initial strain was below the fracture strain of the fibers. However, because the samples were sheet specimens and compressive strains could not be imposed, testing was limited to zero-tension loading. For the NiAl matrix-only samples, accumulated tensile strains were extremely small, being less than 0.35 percent after 100 000 cycles. Finally, Cullers and Antolovich (ref. 20) have performed fully reversed low cycle fatigue testing of polycrystalline NiAl at isothermal temperatures between 600 and 700 K at plastic strain ranges of 0.5 and 1 percent. These tests were performed very near the BDTT of the material, and fatigue lives were limited to 1000 to 3000 cycles, with life at the lower temperatures limited by the presence of internal defects. An analysis of the cyclic deformation behavior and resulting dislocation structures for this material is forthcoming (ref. 21).

Limited room-temperature low cycle fatigue data also exist for other B2 compounds, namely FeCo-2V (ref. 22), Fe-40Al (refs. 23 and 24), and Ni-20Fe-30Al (refs. 23 and 24). The extremely poor

fatigue life of the latter two intermetallic alloys combined with the scarcity of data for NiAl raises concerns about the room-temperature fatigue life of NiAl. Also, the lack of fatigue data for temperatures above the BDTT leaves the cyclic behavior of polycrystalline NiAl in this regime unexplored. Consequently, a detailed study of the fully reversed, strain-controlled fatigue behavior of polycrystalline NiAl was performed, and the results at 300 and 1000 K are described.

MATERIAL

Vacuum atomized -20/+325 mesh prealloyed powders of stoichiometric NiAl were obtained from Homogeneous Metals, Inc, Clayville, N.Y. The powders were from heat number P1418, which is the same heat number of the powder being used in a companion fatigue study by Cullers et al. (refs. 20 and 21). The chemical analysis of the powder is shown in table I. The powder was packed in cans of 304 stainless steel approximately 96 mm in diameter by 150 mm in length. The cans were evacuated and hot isostatically pressed (HIP'ed) at 1533 K and 241 MPa pressure for 5 hr. These HIP conditions are essentially the minimum necessary to produce full consolidation while minimizing time at temperature (ref. 25) and are similar to the final processing step for continuous fiber, NiAl-based composites produced by the powder cloth technique (ref. 26). The as-received microstructure for the HP NiAl is shown in figure 1. Prior powder particle boundaries are often observed. Grain size distribution was measured (fig. 2) as recommended in ASTM standards E112 and E1181. The mean grain size was 70 ± 14 μm.

Cast-and-extruded (C+E) NiAl was produced by vacuum induction melting commercially pure Ni and Al at the equiatomic composition and casting it into copper chill molds. Average values of post-extrusion chemical analyses of the NiAl samples are presented in table I. Two cropped NiAl ingots, nominally 38 mm in diameter and 95 mm in length, were canned in mild steel and extruded at 1200 K at an area reduction ratio of 12:1. The resulting material consisted of equiaxed grains (fig. 3) of 18 ± 3 μm. The grain size (fig. 4) varied much less than that in the HP material (fig. 2).

EXPERIMENTAL PROCEDURE

Since the brittle-to-ductile transition temperature (BDTT) of the HP NiAl was unknown, uniaxial tensile testing was performed on cylindrical buttonhead specimens with typical gauge diameters of 3.2 mm and lengths of 30 mm. Each specimen was electropolished in a 10-percent perchloric acid–90-percent methanol solution prior to testing. Tensile tests to failure were performed in a universal testing machine under displacement control at isothermal temperatures between 500 and 1000 K and initial strain rates of 1.4×10^{-4} and 1.4×10^{-3} sec^{-1}. A resistance-heated furnace was used for the tensile tests, which were performed in air. The temperature gradient along the gauge section of the tensile samples was within ±2 K at all temperatures. Stress-strain data were obtained from the load-time plots.

For fatigue samples, 13-mm-diameter by 114-mm-long cylindrical specimens (fig. 5) were ground from the extruded bars or the electrodischarge-machined blanks of HP. To allow deformation and damage to be easily observed, the reduced gauge section of each specimen was similarly electropolished in a 10-percent perchloric acid–90-percent methanol solution at 20 to 25 V, 1 A, and -65 °C prior to testing. The specimens were subsequently dye penetrant inspected, and only specimens which did not show indications of cracks were tested.

The specimens were tested at 300 and 1000 K (1341 °F) in a closed-loop, servohydraulic load frame. The specimen was gripped by 13-mm-diameter collets inserted in water-cooled, hydraulically actuated grips. A clamping force of approximately 125 kN was determined to be sufficient to eliminate slippage of the specimens in the grips without cracking the specimen in the grip area. Strain was measured by using a 13-mm gauge length, clip-on, water-cooled extensometer, which utilized alumina probes to allow testing at elevated temperatures. A spring-loaded system kept the extensometer against the specimen and prevented the probes from slipping. A total spring force of 600 g was used and was found to keep bending of the specimens within acceptable limits at elevated temperatures. Specimens were heated with an induction coil powered by a 5-kW radio frequency heater. Temperature was measured and controlled by an infrared pyrometer, since the notch sensitivity and brittleness of this material precluded the welding of thermocouples onto a test specimen. To determine the temperature gradient along the gauge length, three thermocouples were spot welded along the gauge length of a dummy NiAl specimen. The pyrometer was also calibrated to this thermocoupled specimen. The temperature gradient was no more than 5 K at the test temperature of 1000 K.

Specimens were subjected to either monotonic tension or low cycle fatigue loading. In both cases, the loading was applied at a constant total strain rate of 10^{-3}/s. The fatigue specimens were cycled in a fully reversed fashion between constant plastic strain, ε_p, limits. These limits were calculated by subtracting the elastic portion of the strain, σ/E, from the total strain, ε_t, as follows:

$$\varepsilon_p = \varepsilon_t - \sigma/E \tag{1}$$

where σ is the stress and E is the modulus of the specimen, as determined prior to the start of the test. The plastic strain was calculated, and the total strain was subsequently adjusted each cycle by the computer, which also collected stress and strain data.

After failure of the specimen (i.e., breaking into two separate pieces), representative fracture surfaces were examined with the scanning electron microscope (SEM). Subsequently, longitudinal cross sections were cut from the samples, metallographically prepared, and examined by optical microscopy to determine damage modes. Selected polished samples were also examined with the SEM.

RESULTS

Tests at 300 K

The cast-and-extruded (C+E) material was tested both in monotonic tension and under cyclic loading at 300 K. Figure 6 shows the 300 K stress-strain behavior for a C+E sample whose tensile properties are given in table II. The elastic modulus was 240 GPa, which is identical to that determined by an ultrasonic technique (ref. 27); yielding occurred at a stress of 216 MPa. The specimen exhibited a distinct yield point and a Luder's regime, followed by slight hardening. Failure occurred at 270 MPa and at a strain of 0.85 percent.

The C+E samples were fatigued at plastic strain ranges of 0.06 to 0.2 percent. The fatigue data for each specimen are listed in table III. In this table, $\Delta\varepsilon_p$ is the plastic strain range, and N_f is the fatigue life of the specimen defined as fracture or separation into two distinct pieces. The total strain range $\Delta\varepsilon_t$ and the stress range $\Delta\sigma$ were taken at halflife $N_f/2$, since the specimens were cycled between constant plastic strain limits and $\Delta\varepsilon_t$ and $\Delta\sigma$ varied as a function of cycle.

The 300 K fatigue life for the C+E samples is plotted in figure 7 as a function of the plastic strain range. On a log-log plot, a straight line is typically fit to the data, as discussed in reference 28. A least squares analysis of the NiAl data yields the following life relationship:

$$\Delta\varepsilon_p = 0.0032\ N_f^{-0.14} \tag{2}$$

When fatigue life is plotted on a stress range basis (fig. 8), the log-log plot shows a similar linear relationship. A straight line fitted to these data yields the following form:

$$\Delta\sigma\ (\text{MPa}) = 758\ N_f^{-0.0045} \tag{3}$$

where $\Delta\sigma$ is the stress range (in MPa) taken at halflife ($N_f/2$). Note that the stress datapoint for specimen C_14 lies much below the curve. This specimen was found to have a large pore (fig. 9) that initiated cracking and caused premature failure. For this reason, equation (3) was calculated without this datapoint. This specimen ($N_f = 269$) and specimen C_13 ($N_f = 929$) were both tested at the same strain range of 0.1 percent. Since the C+E material hardens substantially during cyclic loading, premature failure will not allow the stress range to reach its fully hardened value. In fact, if the stress range of specimen C_13 (560 MPa) at 250 cycles is compared with that of specimen C_14 at failure (269 cycles), they are found to be nearly identical. Thus, had specimen C_14 not failed prematurely, its stress level probably would have reached the 700 MPa range.

Figure 10, which depicts a set of hysteresis loops taken at various cycles, illustrates that at 300 K the specimens harden continuously during cyclic loading without reaching saturation. It should be noted that in the loop for cycle one there is a distinct yield point similar to that which occurs during tensile testing (fig. 6). This yield point is also present in the compressive portions of the loop and in subsequent cycles, although to a much lesser extent. The cyclic hardening is also depicted in figure 11, where the absolute values of the C_15 specimen's tensile and compressive stress amplitudes are plotted as a function of cycles. This specimen hardened to twice its initial value in just 400 cycles and exceeded the ultimate tensile strength for the monotonic test after only 40 cycles. The stress values in tension and compression are approximately equal in the beginning of the test, but the absolute compressive stress quickly exceeds the tensile stress and remains larger throughout the rest of the life.

The cyclic stress-strain curve (at halflife) is shown in figure 12. Again, the least squares fit was determined without the data from specimen C_14, which fell significantly below the other points on the curve. The equation is

$$\Delta\sigma\ (\text{MPa}) = 906\ \Delta\varepsilon_p^{0.031} \tag{4}$$

Tests at 1000 K

Both the C+E and the HP NiAl were fatigue tested at 1000 K. This temperature is well above the BDTT for both the C+E (ref. 11) and the HP NiAl samples, as demonstrated in figure 13. Above the BDTT, both materials exhibit extensive tensile ductility before fracture. The initial portion of their monotonic tensile stress-strain behavior is shown in figure 14, and the tensile properties are given in table II. The HP material is 40 percent stronger than the C+E material. Moreover, each material exhibits a yield point similar to that observed at 300 K (see fig. 14). The tensile tests were terminated long before failure occurred since the failure strains are very large (>25 percent) and the large displacement could have

damaged the extensometer. The elastic moduli given in table II for both materials are similar to those measured by an acoustic resonance method (ref. 29) on corresponding hot pressed or extruded material. They are, however, approximately 20 percent lower than values obtained by using an ultrasonic technique (ref. 27). But the material in that study was processed differently, and the modulus of NiAl is known to be sensitive to texture and thus to the processing technique used (ref. 2).

The 1000 K fatigue life of the HP and the C+E samples is plotted in figure 15 as a function of plastic strain range. The C+E material has a life approximately three times longer than that of the HP. When the HP specimens were tested in vacuum (1.3×10^{-4} Pa), their lives lengthened by a factor of three, equaling those of the air-tested C+E material, at least at the higher plastic strain ranges. At plastic strain ranges of 0.3 percent and higher, a slope of -0.7 was calculated for the HP samples by least squares analysis. The same slope was calculated for the C+E data. This slope is close to the value of -0.6 commonly used in the universal slopes equation for predicting fatigue life (ref. 28). At lower plastic strain ranges the fatigue life of the HP specimens drops off and the life curve takes a downward trend. There is a large amount of scatter in the data at the lower strain ranges, and therefore, the life curve was sketched in just to indicate a general trend. The C+E data do not appear to have the downward trend at lower plastic strain ranges, although more tests would be needed for confirmation. The life line for the vacuum data was assumed to be the same as that for the air, and therefore, the air curve was simply translated to the longer lives exhibited by the vacuum tests. Similar life line curves can also be observed in the total strain range (at halflife) plotted as a function of life in figure 16.

A comparison of the life of the C+E material tested at the two different temperatures is shown in figure 17. At large strain ranges the material has a far superior fatigue life at 1000 K than at 300 K, when examined on a plastic strain range basis. However, just the opposite is true on a stress range basis, as depicted in figure 18. The stress levels of the HP material (fig. 18) are intermediate to the 300 K and 1000 K C+E values. Note that the sharp dropoff in the HP material's life line shown in figures 15 and 16 does not occur in figure 18 in the plot on a stress range basis.

The flow behavior of NiAl at 1000 K is represented by the hysteresis loops shown in figure 19. These loops represent the first cycle of a C+E and of an HP specimen tested at a plastic strain range of 0.50 percent. Jerky flow was observed for the C+E material during the first load-up (as evidenced by the jagged appearance in the loop) and for subsequent cycles. This may be due to dynamic recrystallization, which has been observed during hot tensile testing of a NiAl alloy at similar temperatures (ref. 30). In both tension and compression and for all subsequent cycles, discontinuous yielding was observed. Yield points occurred at approximately 0.001 plastic strain after each load reversal; therefore, for tests run at a plastic strain range of 0.0006, the yield point in the tension portion of the loop was missing and was evident only in the compression portion of the loop.

Unlike the specimens tested at 300 K, the specimens tested at 1000 K hardened slightly then softened to failure (fig. 20). As at 300 K, the compressive stresses were generally larger than the tensile stresses. The C+E material and the air-tested HP samples reached their peak hardness at less than 1 percent of their total life. The HP samples tested in vacuum hardened nearly to failure. Although the samples hardened or softened at 1000 K, the amount of hardening and softening was very small. The largest change in the stress was approximately 35 MPa, which was much smaller than the 200 to 300 MPa increase for the specimens tested at 300 K.

The cyclic stress-strain behavior at 1000 K is shown in figure 21. All data from the HP samples are clustered together and lie significantly above those of the C+E material. This is due to the higher yield stress of the HP samples. Least squares fits for the two types of material yielded the following equations:

$$\Delta\sigma \text{ (MPa)} = 507\ \Delta\varepsilon_p^{0.12} \quad \text{(HP)} \tag{5}$$

$$\Delta\sigma \text{ (MPa)} = 174\ \Delta\varepsilon_p^{0.062} \quad \text{(C+E)} \tag{6}$$

OBSERVATIONS OF DAMAGE

Tests at 300 K

At 300 K the C+E samples failed in an intergranular manner. The fracture surface was relatively featureless (fig. 22), primarily because of the small grain size and the brittle fracture behavior. Only at this temperature were specific initiation sites observed in every specimen. Internal defects (fig. 9) in the form of large voids with a teardrop-shaped cross section were present in the C+E material (fig. 23) as stringers, which were aligned parallel to the extrusion axis. Despite the 12:1 reduction ratio during extrusion, this material remained unconsolidated, probably owing to the presence of entrapped gas. These voids were typically smaller ($\sim 20 \times 20\ \mu$m) than the one shown in figure 9, which was particularly large and led to the premature failure of specimen C_14. Although these processing defects were also present in the C+E samples tested at 1000 K, they did not appear to initiate nor influence cracking or fatigue behavior at this temperature, probably because of the material's high ductility and toughness at elevated temperatures.

The specimens tested at 300 K contained very few secondary cracks, again indicating the brittleness of the material. The secondary cracking that was observed was concentrated near the fracture surface (fig. 24) and was probably a result of the final overload failure of the sample. An enlargement of these secondary cracks shows primarily intergranular cracking (fig. 25), with some crack-stringer interaction.

Tests at 1000 K

HIP'ed prealloyed powder.–The NiAl HP specimens tested at 1000 K failed primarily through slow, stable intergranular crack growth. Instances of faster crack growth were typified by transgranular cleavage fracture. In general, fatigue cracking initiated at multiple locations along the specimen surface. Specific anomalies that could be associated with initiation were difficult, if not impossible, to locate. Occasionally, an identifiable initiation site could be observed, such as the one indicated in figure 26 for a specimen tested at a high plastic strain range. This initiation area is characterized by large sections of cleavage failure emanating radially from an area of approximately 0.5 mm in diameter.

In specimens tested in air at 1000 K, fatigue crack growth was marked by a dark oxide trail. This oxide can be seen in figure 27(a), where, for a specimen tested at a high plastic strain range, the fatigue crack occupies a very small portion ($\sim$20 percent) of the cross-sectional area (fig. 27(b)). At lower strain ranges, the fatigue crack occupied a much larger percentage ($\sim$50 percent) of the cross-sectional area (fig. 28, parts (a) and (b)).

Another difference between specimens tested at high and low plastic strain ranges was the amount of deformation and secondary cracking observed on the gauge surface. At high plastic strain ranges (fig. 29), significant cracking, predominantly intergranular, was observed on the gauge surface. The grains also were often roughened by plastic deformation. This is in contrast to specimens tested at low plastic strain ranges (fig. 30), where there is minimal secondary cracking on the gauge surface and little evidence of plastic deformation on the sample surface. These results were not unexpected since the response stress is on the order of the yield stress (~100 MPa) at lower plastic strain ranges.

Metallographic sections taken from specimens tested at 1000 K revealed numerous intergranular cracks that originated at the gauge surface. In addition, a high percentage of the grain boundaries were decorated with tiny pores or voids, which are typical of diffusional creep damage (fig. 31). Such porosity was observed at all plastic strain ranges.

Fracture surfaces for the specimens tested in vacuum were similar to those tested in air. Cracking was predominantly intergranular (fig. 32), and this cracking extended over most of the specimen. The larger extent of slow fatigue crack growth in vacuum compared to air probably contributed to the longer life and is indicative of an environmentally assisted fatigue damage mechanism.

Cast and extruded.–The C+E specimens fractured intergranularly at 1000 K, and fatigue crack growth existed over approximately 80 percent of the specimen fracture surface regardless of the applied plastic strain range (figs. 33 and 34). At high plastic strain ranges, more secondary intergranular cracking and damage (fig. 35) was observed on the gauge surface in comparison to the specimens tested at low plastic strain ranges (fig. 36). The fracture surfaces of many C+E specimens showed regions in which an individual grain stuck out from the sample surface and was surrounded by a "moat"-like empty region, resulting in dark shadows as seen in figure 33(b). Enlargements of these areas showed individual grains (fig. 37) which were torn from the sample surface and were only loosely connected with the bulk of the specimen. Subsequent metallographic sections (fig. 38) revealed that several grains were missing throughout the gauge. They were probably substantially damaged during the fatigue process and pulled out during metallographic preparation. These observations demonstrate the high degree of intergranular fatigue damage that occurred in the NiAl samples at 1000 K.

Figure 39, as well as figures 33 and 34, illustrates that after 1000 K fatigue testing, the grain size of the C+E material was ~75 μm. This is four times larger than the 18 μm grain size observed in the as-received specimens. Exposure to temperature at 1000 K in an unstressed condition was not sufficient to cause grain growth. The as-received grain size (fig. 40(a)) remains unchanged after an 80 h-1000 K heat treatment (fig. 40(b)), which simulates the longest fatigue test time. On the other hand, the fatigue tested sample (fig. 40(c)) underwent considerable grain growth. (Note: The grain size in the HP material did not change during testing, since the grain boundaries were pinned by prior powder particle boundaries.) This indicates that temperature alone is not sufficient to cause grain growth; both heat and plastic deformation are required. In addition to causing grain growth in C+E samples, fatigue also produced a high density of grain boundary pores (fig. 39) similar to those observed in the HP specimens. These pores were found throughout the gauge section and provided a means of easy crack propagation from grain to grain.

DISCUSSION

Behavior at 300 K

The 300 K fatigue behavior of NiAl can be better understood by comparing and contrasting the cyclic deformation of this intermetallic to the monotonic behavior. From investigations of the monotonic flow and fracture of NiAl (refs. 4, 10 to 12, 15, and 32), it is evident that the 300 K ductility and fracture is controlled by Griffith-like defects generated at the grain boundaries during plastic deformation. The insufficient number of independent slip systems in NiAl (refs. 4, 12, and 15) leads to these defects, which scale with the grain size. Once a critical stress intensity is achieved, the defects propagate catastrophically and result in brittle fracture.

It is apparent that the slip process is largely reversible during fatigue of NiAl, and it is this reversibility which prevents grain boundary defects from being activated. A detailed explanation of the slip process is not possible here, but some speculation can be made. Since slip is planar at 300 K, dislocations can easily reverse their motion under reversed loading. They will meet resistance largely from dislocations on intersecting slip planes or from forest-type dislocations within the grain. A larger stress will be required to move these dislocations past the intersections, thereby resulting in work-hardening. The dislocations are relatively free to move back and forth between intersecting planes, which would account for the large degree of slip reversibility observed in this material. The large degree of slip reversibility is evident from the very low slope in the plastic strain range-life curve (eq. (1)). The slope, $c = -0.14$, is much lower than the value of -0.6 typically found for most metallic materials (ref. 28). In the elastic strain-life curve (eq. (2)), a low slope, $b = -0.0045$, was also observed; this is much lower than the -0.12 value obtained for most metallic materials (ref. 28). In fact, such a low slope is consistent with the fact that the lives of brittle materials can be determined from the presence of certain size defects in relation to the applied stress level. It is unusual that both slopes are so small, yet they are consistent with one another since their ratio, b/c, is equal to the exponent for the cyclic stress-strain curve (eq. (3))—a check which is commonly employed in fatigue investigations (ref. 28).

During fatigue cycling of binary near-stoichiometric NiAl, the material work-hardened to stress levels that were at least 60 percent greater than the monotonic tensile strength of the material. This indicates that, although fracture in binary NiAl is plasticity dependent, cyclic strain in NiAl is easily reversible; thus it is more difficult for damage to accumulate at the grain boundaries because of the slip processes. In other words, at a given strain range, dislocation motion is largely reversible. Failure occurs only after the stress in the fatigue sample, due to work-hardening, increases to a level that causes fracture to initiate at some current defect, as opposed to forming a critical defect at the grain boundaries as in monotonic deformation.

To help clarify the damage mechanisms due to monotonic versus cyclic strain, a runout fatigue sample (102 000 cycles at a plastic strain range of 0.06 percent) was subsequently deformed in tension to failure (fig. 6). The modulus of this specimen was identical to the as-received material. However, the specimen had work-hardened considerably during fatigue testing (e.g., fig. 11) and, therefore, under monotonic loading failed in tension at 380 MPa. The ultimate tensile strength of this prefatigued specimen was approximately 40 percent higher than that of the as-extruded sample. However, this increase in stress-carrying capability was gained at the expense of ductility, as indicated by the lower, 0.3 percent failure strain. In the prefatigued sample, the fracture mode was predominantly intergranular, similar to the as-extruded material; this indicates that noncompatible strain accumulation which results in grain boundary discontinuities still controls the fracture initiation mechanism. During fatigue, the sample

accumulated a strain of over 6000 percent, yet this strain was insufficient to cause significant damage. When the sample was then deformed monotonically, the yield stress was as high as the fracture stress of the as-extruded material (fig. 6), yet the material still exhibited some tensile ductility. The ductility was lower than for the as-extruded material because less additional plastic deformation was needed to activate a grain boundary defect of critical size to cause failure at the higher stress level.

If defect generation at the grain boundaries is less active under cyclic deformation (unlike monotonic deformation), then other flaws in the material are responsible for fracture initiation. In the case of the C+E NiAl tested during this investigation, processing defects or pores (see figs. 9 and 23) were present and apparently became the life-controlling defects in the material. The dependence of fatigue life on these processing defects was especially evident when fatigue life was described on a stress range basis:

$$\Delta\sigma \text{ (MPa)} = 758 \, N_f^{-0.0045} \tag{7}$$

where $\Delta\sigma$ is the stress range taken at halflife $N_f/2$. The small exponent indicates that fatigue life is extremely sensitive to stress over a narrow range of stresses, as is evident in figure 8, and that fatigue failure occurs once this critical stress range in the material is reached. The critical stress is related to the defect size, as manifested by specimen C_14. This specimen (fig. 9) contained an unusually large defect of $\sim$160 μm (a 20-μm defect is typical in all other samples), and therefore it failed prematurely and at a much lower stress level (fig. 8). This behavior is consistent with the low toughness (ref. 13) and high notch sensitivity of the material. Conversely, below this critical stress range and for a given defect size, fatigue loading would be of no consequence and lives should be infinite.

Because cyclic strain is largely reversible in NiAl, even though its monotonic tensile ductility is poor, its 300 K low cycle fatigue life on a plastic strain range basis is comparable or superior to other B2 alloys for which low cycle fatigue data have been reported (refs. 22 to 24). For example, extruded powder processed alloys of Fe-40Al and Ni-30Al-20Fe have tensile ductilities similar to NiAl. However, at a plastic strain range of 0.0002, as-extruded Fe-40Al has a fatigue life of approximately 25 cycles, which can be improved to about 250 cycles through application of prestrain and surface films (refs. 23 and 24). Similarly, at a plastic strain range of 0.0006, as-extruded Ni-30Al-20Fe has a fatigue life of about 300 cycles, which can be increased to nearly 1500 cycles through a combination of prestrain and surface film coatings (refs. 23 and 24). Even though there was significant scatter in the data, at a plastic strain range of 0.0006 the fatigue life for C+E NiAl varied from 20 000 to more than 102 000 cycles, which is several orders of magnitude greater than the B2 alloys studied by Hartfield-Wunsch (refs. 24 and 25). A direct comparison between NiAl and the weakly ordered, more ductile B2 alloy FeCo-2V is difficult, since the latter study was performed between total strain limits (ref. 23). Nevertheless, taking into account the high strength and work-hardening rate of the FeCo-2V alloy, which would result in a small and continuously decreasing plastic strain component during testing, NiAl would seem to have a comparable or superior fatigue life. Furthermore, if the processing defects present in the current NiAl material were eliminated, the fatigue life should be further improved.

Fatigue Behavior at 1000 K

At temperatures in the range of 550 to 700 K and at nominal strain rates on the order of 10^{-4} to 10^{-3}/s, NiAl undergoes a very dramatic change in mechanical behavior, from brittle to ductile (fig. 13). In this range, the fracture strength and tensile ductility for NiAl increase significantly (refs. 10 to 12 and 31); for example, tensile elongations of 20 to 80 percent are common. At the BDTT fracture tough-

ness also changes, increasing from approximately 5 MPa$\sqrt{m}$ to more than 30 MPa$\sqrt{m}$ over this same temperature range (ref. 13). Therefore, since both the C+E and HP NiAl materials tested at 1000 K were well above the BDTT, they exhibited a tensile deformation behavior considerably different from that at 300 K.

The fatigue behavior at 1000 K is also considerably different than that at 300 K. The material is no longer flaw-sensitive since cracks did not initiate from processing defects as they did at 300 K for the C+E material (fig. 9). Also, the lives at 1000 K are longer in the higher plastic strain ranges than they are at 300 K; in fact, the material exhibits the strain range-life behavior typical of most metals. However, at lower plastic strain ranges a change in slope of the strain range-life curve occurs (fig. 15). A downward trend in the fatigue curve at low plastic strain ranges, although unusual, has been observed; for example, in a magnesium alloy (ref. 32) that experienced grain boundary cracking. The grain boundary cracks reduced the effective cross-sectional area of the specimen, thereby increasing the crack growth rate and leading to premature failure. Beere and Roberts (ref. 33) proposed a similar behavior, in which the life of the specimen depends on two competing damage mechanisms: fatigue crack growth and grain boundary cavity growth. At high plastic strain ranges, the specimen fails by fatigue crack growth. At lower strain ranges, cavity growth dominates and the life curve has a downward trend.

At 1000 K the deformation behavior of binary NiAl is characterized by dislocation creep processes controlled by dislocation climb (refs. 2 and 18), even at a strain rate as high as 1×10^{-3} (refs. 16 and 17). Because most testing of NiAl (refs. 16 to 18) has been in compressive creep, topics such as grain boundary cavitation, necking, and tertiary creep have not been adequately addressed. It is apparent from this study, however, that grain boundary cavitation is a principal mechanism of damage in fatigue samples tested at 1000 K and that at low plastic strain ranges the continued growth of these cavities results in failure at anomalously low lives.

The fatigue life curve in figure 15 indicates that the C+E material exhibits a factor-of-three longer fatigue life at 1000 K than the HP NiAl. One possible explanation is that the yield stress and cyclic response stress of the C+E material are approximately a factor of two lower than those of the HP material. As such, the crack driving force would be significantly smaller in the C+E material, thereby resulting in a longer life.

By testing samples in air versus vacuum, we found that environment plays a part in limiting the fatigue life of NiAl at 1000 K. The fatigue lives of the HP material tested in vacuum increased by a factor of three compared to air. This increase in fatigue life could be a result of decreased fatigue crack growth rates in vacuum. In air, oxidation of the intergranular surface cracks would accelerate crack growth rates, presumably by lowering the surface free energy (ref. 34). A similar effect of environment has been observed in the fatigue life of copper (refs. 35 and 36) and other material systems (ref. 37). The environment may also shorten fatigue life through an embrittlement of the bulk material. This would explain why the fatigue crack in a vacuum-tested sample covered a larger percentage of the fracture surface than it did in air-tested samples. A crack in oxygen-embrittled, air-tested material would reach its critical length in a shorter distance than would a crack in the more ductile, vacuum-tested specimens. The actual mechanism behind this embrittlement is currently unknown.

The fatigue life of NiAl has been compared to the lives of various turbine disk and blade alloys at temperatures of approximately 1000 K. The following nickel-base superalloys were used for comparison: Waspaloy (ref. 38), René 95 (ref. 38), single crystal René N4 (ref. 39), and directionally solidified MAR-M246 (ref. 40). The NiAl material in both the HP and C+E form had superior fatigue properties when

compared on a plastic strain range basis (fig. 41). However, on a stress range basis, NiAl was inferior to the superalloys (fig. 42). Note in figure 42 that the superalloy data are bounded by René 95 and Waspaloy. All the other alloys and conditions from figure 41 fall between these two life lines, but were omitted for clarity. The reason that NiAl performs poorly (see fig. 42) is that its yield stress is low (~100 MPa) compared to yield stresses of 600 to 1000 MPa for the superalloys. Alloying additions could raise the strength of NiAl (refs. 2, 12, and 31), but at the expense of the ductility. Although the current NiAl material does not have adequate strength to be used in a monolithic form, it would make an excellent matrix material for a composite; then the fibers could carry the load, and the NiAl matrix would contribute its excellent strain cycling capabilities and oxidation resistance.

SUMMARY OF RESULTS

The low cycle fatigue behavior of polycrystalline NiAl was studied at 300 and 1000 K. The following results were obtained:

1. The fully reversed, plastic strain-controlled fatigue behavior of cast and extruded (C+E) NiAl was evaluated at 300 K for plastic strain ranges of 0.0006 to 0.002. Except at the smallest plastic strain range investigated, NiAl work-hardened continuously until failure, with a final fracture stress 60 percent greater than its ultimate tensile strength.

2. Fatigue fracture initiation at 300 K occurred at large internal teardrop-shaped pores. However, the majority of the fracture surface was intergranular in nature, consistent with the limited number of operative slip systems in NiAl.

3. Compared on a plastic strain range basis, C+E NiAl has a much greater fatigue life at 300 K than comparable B2 ordered compounds.

4. The fatigue life of NiAl is limited by low ductility and toughness at 300 K. At 1000 K, plastic deformation due to poor creep resistance led to a lowered fatigue life at low plastic strain ranges.

5. The fatigue life for C+E NiAl is a factor of three greater than for HIP'ed powder (HP) NiAl at 1000 K, because of its lower response stress and consequently lower crack-driving force.

6. Fatigue testing the HP NiAl in vacuum improves its fatigue life by a factor of three compared to air testing.

7. Fatigue crack growth in both the C+E and the HP NiAl samples was almost completely intergranular and was a result of the extensive grain boundary void formation at 1000 K.

8. The grain size in the C+E NiAl increased during testing at 1000 K. Plastic deformation was found to be necessary to cause grain growth. The grain size in the HP NiAl remained unchanged during testing, since the grain boundaries were pinned by prior powder particle boundaries.

9. NiAl exhibited a superior fatigue life at 1000 K when compared on a plastic strain range basis to superalloys, but it was inferior to the superalloys on a stress basis. The poor performance of NiAl on a stress range basis is due to its low yield strength compared to the superalloys.

ACKNOWLEDGMENTS

The authors wish to acknowledge the many helpful discussions with Drs. G.R. Halford and J.D. Whittenberger of NASA Lewis Research Center and the experimental support of R. Corner of Sverdrup Technologies, Inc., Lewis Research Center Group.

REFERENCES

1. Darolia, R.: NiAl Alloys For High Temperature Structural Applications. J. Met., vol. 43, no. 3, 1991, pp. 44–49.

2. Noebe, R.D.; Bowman, R.R.; and Nathal, M.V.: Review of the Physical and Mechanical Properties of the B2 Compound NiAl. NASA TM-105598, 1992.

3. Rozner, A.G.; and Wasilewski, R.J.: Tensile Properties of NiAl and NiTi. J. Inst. Met., vol. 94, 1966, pp. 169–175.

4. Ball, A.; and Smallman, R.E.: The Operative Slip System and General Plasticity of NiAl - II. Acta Metall., vol. 14, 1966, pp. 1517–1526.

5. Law, C.C.; and Blackburn, M.J.: Rapidly Solidified Lightweight Durable Disk Material. Final Report AFWAL-TR-87-4102, 1987.

6. Cotton, J.D., et al.: The Potential for Room Temperature Ductility in Polycrystalline NiAl Through Slip System Modification by Macroalloying. HITEMP Review 1991: Advanced High Temperature Engine Materials Technology Program, NASA CP-10082, 1991, pp. 23–1 to 23–18.

7. George, E.P.; and Liu, C.T.: Brittle Fracture and Grain Boundary Chemistry of Microalloyed NiAl. J. Mater. Res., vol. 5, Apr. 1990, pp. 754–762.

8. Hahn, K.H.; and Vedula, K.: Room Temperature Tensile Ductility in Polycrystalline B2 NiAl. Scr. Metall., vol. 23, June 1989, pp. 7–12.

9. Nagpal, P.; and Baker, I: The Effect of Grain Size on the Room Temperature Ductility of NiAl. Scr. Metall. Mater., vol. 24, Dec. 1990, pp. 2381–2384.

10. Noebe, R.D., et al.: Flow and Fracture Behavior of NiAl in Relation to the Brittle-To-Ductile Transition Temperature. High Temperature Ordered Intermetallic Alloys IV, L. Johnson, D.P. Pope, and J.O. Stiegler, eds., MRS Symposia Proceedings, Vol. 213, MRS, Pittsburgh, PA, 1991, pp. 589–596.

11. Noebe, R.D.; Cullers, C.L.; and Bowman, R.R.: The Effect of Strain Rate and Temperature on the Tensile Properties of NiAl. J. Mater. Res., vol. 7, Mar. 1992, pp. 605–612.

12. Bowman, R.R., et al.: Correlation of Deformation Mechanisms with the Tensile and Compressive Behavior of NiAl and NiAl (Zr) Intermetallic Alloys. Metall. Trans. A, vol. 23A, May 1992, pp. 1493–1508.

13. Reuss, S.; and Vehoff, H.: Temperature Dependence of the Fracture Toughness of Single Phase and Two Phase Intermetallics. Scr. Metall. Mater., vol. 24, June 1990, pp. 1021–1026.

14. Vehoff, H.: Fracture Mechanisms in Intermetallics. Ordered Intermetallics - Physical Metallurgy and Mechanical Behavior, C.T. Liu, et al., eds., NATO ASI Series E, Vol. 213, Kluwer Academic Publishers, 1992, pp. 299–320.

15. Ball, A.; and Smallman, R.E.: The Deformation Properties and Electron Microscopy Studies of the Intermetallic Compound NiAl. Acta Metall., vol. 14, 1966, pp. 1349–1355.

16. Whittenberger, J.D.: Effect of Composition and Grain Size on Slow Plastic Flow Properties of NiAl Between 1200 and 1400 K. J. Mater. Sci., vol. 22, Feb. 1987, pp. 394–402.

17. Whittenberger, J.D.: The Influence of Grain Size and Composition on 1000 to 1400 K Slow Plastic Flow Properties of NiAl. J. Mater. Sci., vol. 23, Jan. 1988, pp. 235–240.

18. Nathal, M.V.: Creep Deformation of B2 Aluminides. Ordered Intermetallics - Physical Metallurgy and Mechanical Behavior, C.T. Liu, et al., eds., NATO ASI Series E, Vol. 213, Kluwer Academic Publishers, 1992, pp. 541–563.

19. Bowman, R.R.: Influence of Interfacial Characteristics on the Mechanical Properties of Continuous Fiber Reinforced NiAl Composites. Intermetallic Matrix Composites II, D.B. Miracle and J.A. Graves, eds., MRS Symposia Proceedings, Vol. 273, MRS, Pittsburgh, PA, 1992, pp. 145–155.

20. Cullers, C.L.; and Antolovich, S.D.: Low Cycle Fatigue of NiAl Deformed Near the Brittle-to-Ductile Transition Temperature. Superalloys 1992, S.D. Antolovich, ed., The Metallurgical Society, Inc., Warrendale, PA, 1992, pp. 351–359.

21. Cullers, C.L.: Deformation Mechanisms in Cyclically Deformed NiAl Near the Brittle-to-Ductile Transition Temperature. M.S. Thesis, Georgia Institute of Technology, Atlanta, GA, 1992.

22. Stoloff, N.S.; Choe, S.J.; and Rajan, K.: The Influence of Long Range Order on Fatigue Crack Initiation in an FeCo-V Intermetallic Alloy. Scr. Metall. Mater., vol. 26, Jan. 1992, pp. 331–336.

23. Hartfield-Wunsch, S.E.; and Gibala, R.: Cyclic Deformation of B2 Aluminides. High Temperature Ordered Intermetallic Alloys IV, L. Johnson, D.P. Pope, and J.O. Stiegler, eds., MRS Symposia Proceedings, Vol. 213, MRS Pittsburgh, PA, 1991, pp. 575–580.

24. Hartfield-Wunsch, S.E.: Monotonic and Cyclic Deformation Behavior of B2 Aluminides. Ph.D. Thesis, The University of Michigan, Ann Arbor, MI, 1991.

25. Wright, R.N.; Knibloe, J.R.; and Noebe, R.D.: Consolidation of NiAl Powders Using Hot Isostatic Pressing. Mater. Sci. Eng., vol. A141, no. 1, 1991, pp. 79–83.

26. Pickens, J.W., et al.: Fabrication of Intermetallic Matrix Composites by the Powder Cloth Process. NASA TM-102060, 1989.

27. Harmouche, M.R.; and Wolfenden, A.: Temperature and Composition Dependence of Young's Modulus in Polycrystalline B2 Ni-Al. J. Test. and Eval., vol. 15, no. 2, 1987, pp. 101–104.

28. Manson, S.S.: Fatigue: A Complex Subject - Some Simple Approximations. Exp. Mech., vol. 5, July 1965, pp. 1–34.

29. Hellman, J.R., et al.: Interfacial Shear Studies in Sapphire Fiber-Reinforced Niobium and Nickel Aluminide Composites. HITEMP Review 1990: Advanced High Temperature Engine Materials Technology Program, NASA CP-10051, 1990, pp. 41–1 to 41–11.

30. Vedula, K.; and Stephens, J.R.: B2 Aluminides for High Temperature Applications. High Temperature Ordered Intermetallic Alloys II, N.S. Stoloff, ed., MRS Symposia Proceedings, Vol. 81, MRS Pittsburgh, PA, 1987, pp. 381–391.

31. Noebe, R.D.; and Behbehani, M.K.: The Effect of Microalloying Additions on the Tensile Properties of Polycrystalline NiAl. Scr. Metall. Mater., vol. 27, no. 12, 1992, pp. 1795–1800.

32. Wareing, J.; Tomkins, B.; and Sumner, G.: Extent to Which Material Properties Control Fatigue Failure at Elevated Temperatures. Fatigue at Elevated Temperatures, ASTM STP-520, A.E. Carden, A.J. McEvily, and C.H. Wells, eds., ASTM, Philadelphia, PA, 1973, pp. 123–137.

33. Beere, W.; and Roberts, G.: Fatigue Failure by Creep Cavity Growth at High Temperatures. Acta Metall., vol. 30, 1982, pp. 571–580.

34. Basinski, Z.S.; and Basinski, S.J.: Surface-Related Phenomena in Low Amplitude Fatigue of FCC Metals. Scr. Metall. Mater., vol. 26, 1992, pp. 1505–1510.

35. Wadsworth, N.; and Hutchings, J.: The Effect of Atmospheric Corrosion on Metal Fatigue. Philos. Mag., vol. 3, 1958, pp. 1154–1166.

36. Wang, R., et al.: Fatigue of Copper Single Crystals in Vacuum and in Air. Pt. 1: Persistent Slip Bands and Dislocation Microstructures. Mater. Sci. Eng., vol. 65, 1984, pp. 219–233.

37. Solomon, H.D.; and Coffin, L.F.: Effects of Frequency and Environment on Fatigue Crack Growth in A286 at 1100 °F. Fatigue at Elevated Temperatures, ASTM STP-520, A.E. Carden, A.J. McEvily, and C.H. Wells, eds., ASTM, Philadelphia, PA, 1973, pp. 123–137.

38. Characterization of Low Cycle High Temperature Fatigue by the Strainrange Partitioning Method. AGARD CP-243, AGARD, Paris, France, 1978. (avail. NTIS, AD-A059900).

39. Gabb, T.P.; Gayda, J.; and Miner, R.V.: Orientation and Temperature Dependence of Some Mechanical Properties of the Single-Crystal Nickel-Base Superalloy, René N4. Part II: Low Cycle Fatigue Behavior. Metall. Trans., vol. 17A, Mar. 1986, pp. 497–505.

40. Huron, E.S.; and Antolovich, S.D.: Observations of High Temperature Tensile and Cyclic Deformation in a Directionally Solidified Nickel-Base Superalloy. Structure and Deformation of Boundaries, K.N. Subramanian and M.A. Imam, eds., Metallurgical Society, Warrendale, PA, 1985, pp. 185–203.

TABLE I.—COMPOSITION OF NiAl ALLOYS

Specimen		Content, at.%					
Fabrication method	Grain size, μm	Ni	Al	O	C	S	N
HIP'ed powder (heat number P1418)	70±14	[a]50.5±0.2	[a]49.5±0.2	0.028	0.014	<0.002	<0.0006
Cast + extruded	18±3	[b]50	[b]50	.011	.029	.002	<.003

[a]Determined by wet chemical analysis methods, ±0.2 at.% within a 95-percent confidence interval.
[b]Nominal composition.

TABLE II.—TENSILE PROPERTIES OF NiAl

Specimen	Temperature, K	Elastic modulus, E, GPa	Yield stress, $\sigma_{YS_{0.02}}$, MPa	Ultimate tensile strength, MPa	Failure strain, ε_f, percent
HIP'ed prealloyed powder	1000	160	75	---	>[a]10
Cast + extruded	300	240	216	270	.85
Low cycle fatigue[b]	300	220	265	380	.30
	1000	140	67	---	>>[c]1.9

[a]Test was stopped at 10-percent strain.
[b]Prior to tensile testing, specimen was cycled for 102 000 cycles at 300 K at $\Delta\varepsilon_p = 0.06$ percent.
[c]Test was stopped at 1.9-percent strain.

TABLE III.—FATIGUE DATA FOR NiAl

Specimen	Plastic strain range, $\Delta\varepsilon_p$, percent	Fatigue life, N_f, cycles	Environment	Total strain range, $\Delta\varepsilon_t$, percent	Stress range, $\Delta\sigma$, MPa
HIP'ed prealloyed NiAl powder at 1000 K					
SN 5	1.00	1 119	Air	1.19	275
SN 6	.70	1 828	↓	.88	263
SN 7	↓	(a)	↓	.90	271
SN 8	↓	1 631	↓	.89	267
SN 15	↓	1 353	↓	.89	301
SN 16	.50	2 536	↓	.70	292
SN 17	.20	4 290	↓	.39	254
SN 18	.10	4 345	↓	.27	236
NO_2	.10	11 088	↓	.27	228
NO_3	.50	2 548	↓	.68	270
NO_5	.06	4 395	↓	.19	205
NO_7	.06	8 662	↓	.18	205
NO_10	.50	6 011	Vacuum	.71	260
NO_11	.12	12 158	↓	.26	196
NO_12	.11	14 327	↓	.26	197
NO_13	.22	10 735	↓	.39	234
NO_14	.22	7 550	Air	.37	221
NO_15	.50	3 187	Air	.70	254
Cast + extruded NiAl at 1000 K					
C_6	0.10	48 090	Air	0.17	112
C_3	.20	14 408	↓	.29	121
C_7	.50	(b)	↓		
C_8	↓	(c)	↓		
C_10	↓	9 918	↓	.55	122
C_11	.70	3 958	↓	.79	129
Cast + extruded NiAl at 300 K					
C_13	0.10	929	Air	0.46	738
C_14	.10	269	↓	.37	553
C_15	.20	407	↓	.64	737
C_16	.06	20 273	↓	.44	702
C_17	.06	102 204	↓	.39	713
C_18	.08	54 350	↓	.44	744

[a]Interrupted at 738 cycles.
[b]Interrupted at 785 cycles.
[c]Interrupted at 2248 cycles.

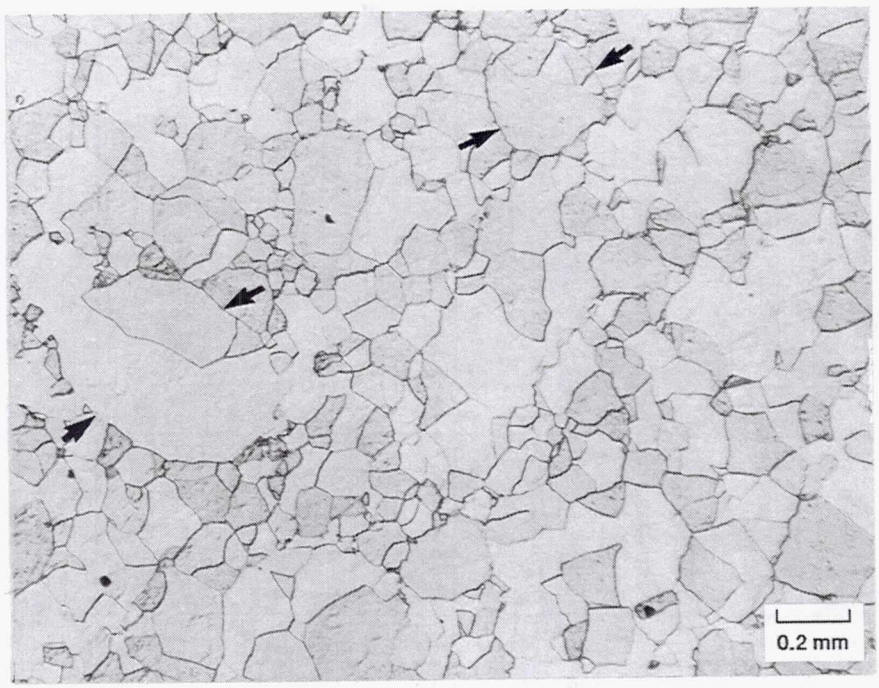

Figure 1.—Optical micrograph of typical microstructure for HP NiAl. Arrows indicate prior powder particle boundaries. Etchant: Kalling's.

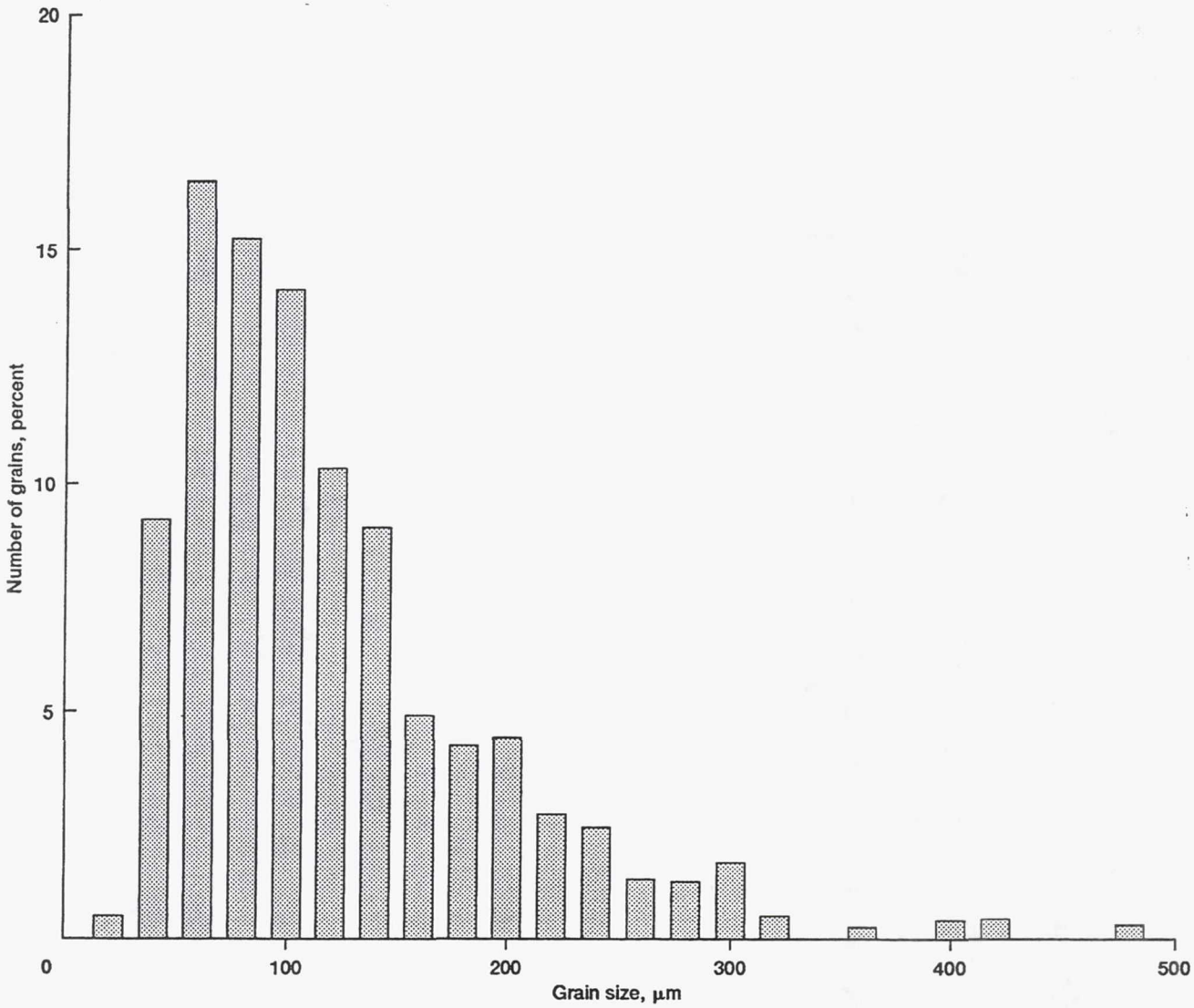

Figure 2.—Grain size distribution of HP NiAl.

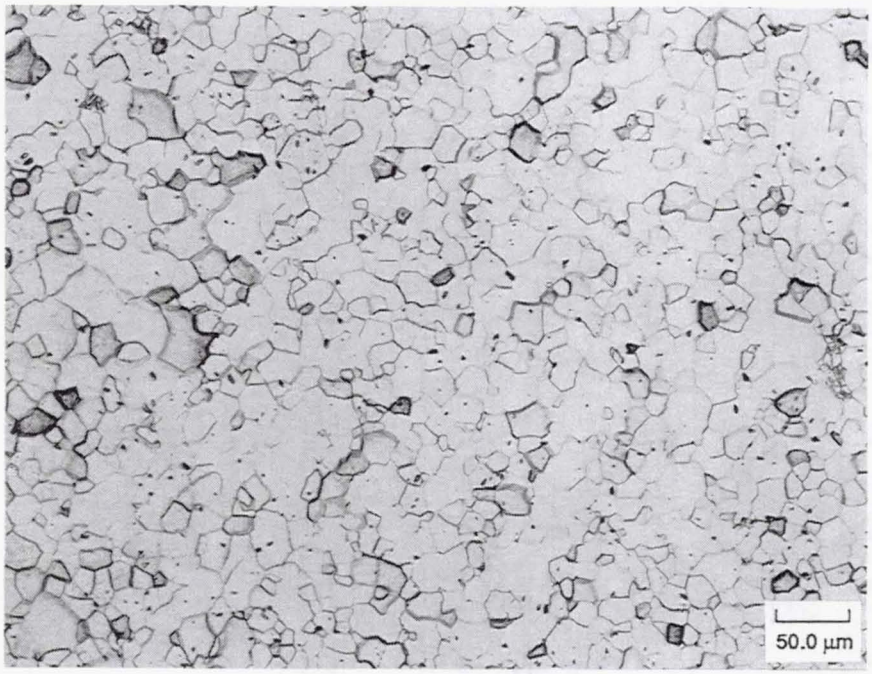

Figure 3.—Optical micrograph of typical microstructure for C+E NiAl. Etchant: Kalling's.

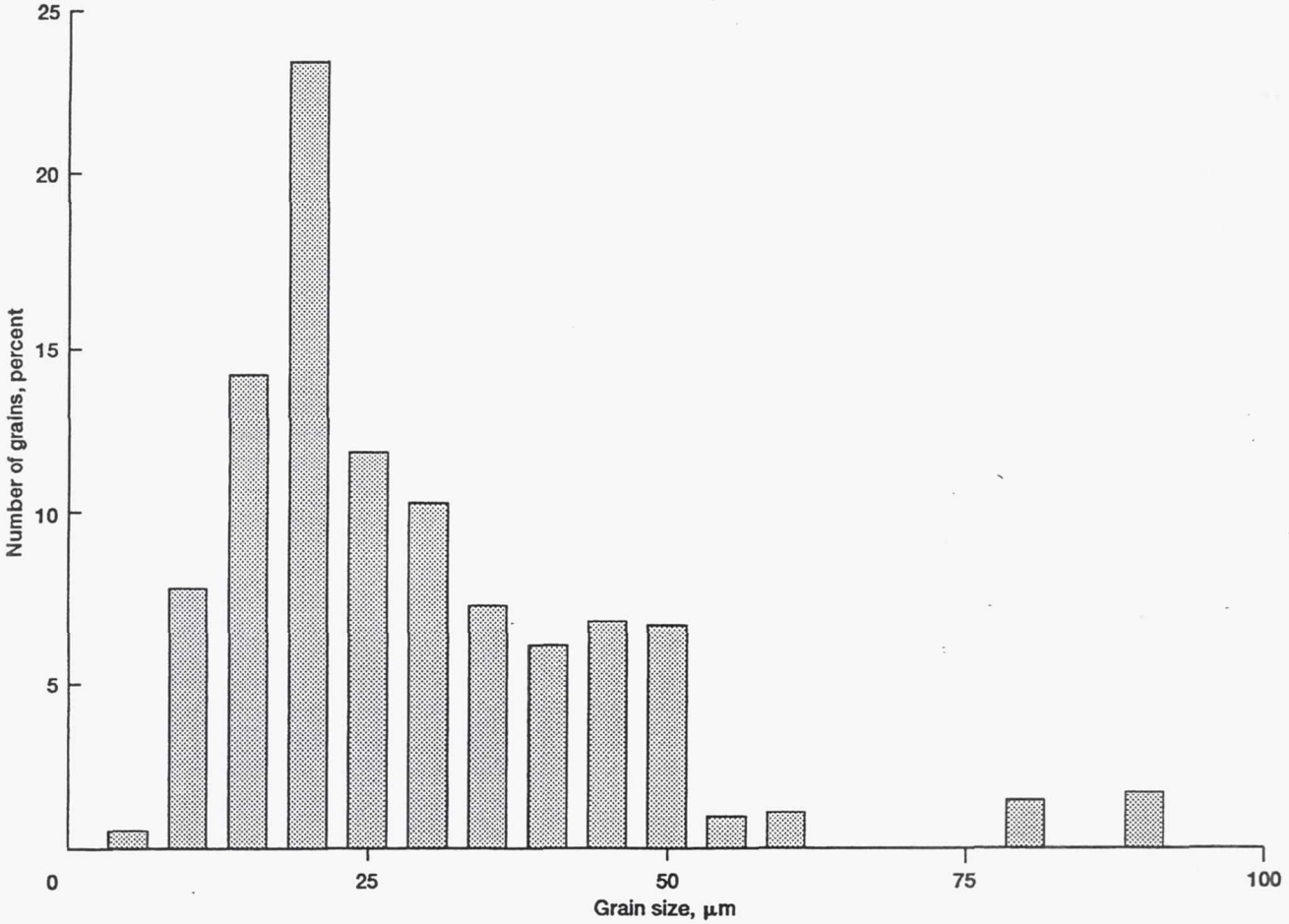

Figure 4.—Grain size distribution of C+E NiAl.

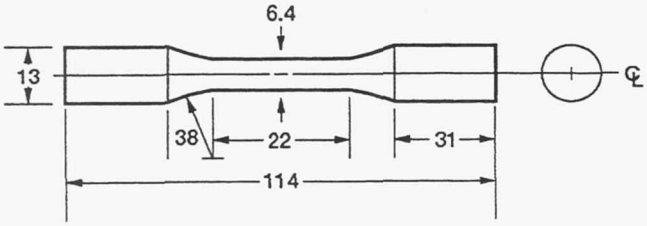

Figure 5.—Geometry of fatigue specimen (all dimensions are in millimeters).

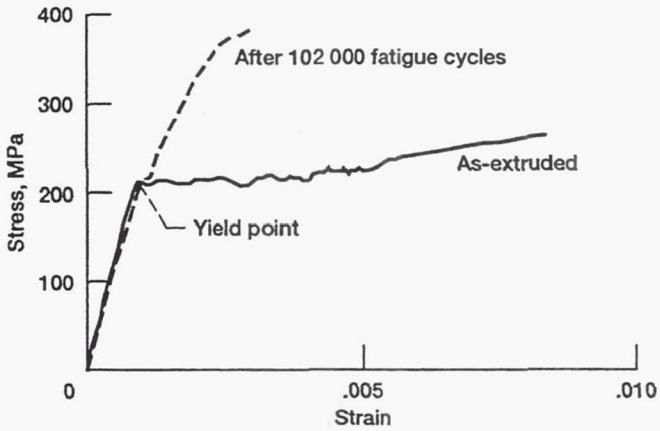

Figure 6.—Tensile curves at 300 K for as-extruded material and prefatigued specimen (102 000 cycles; $\Delta\epsilon_p$ = 0.06 percent).

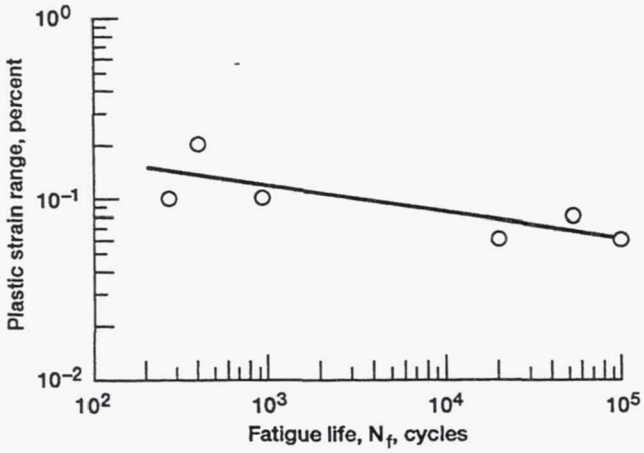

Figure 7.—Fatigue life-plastic strain range curve for C+E material tested at 300 K.

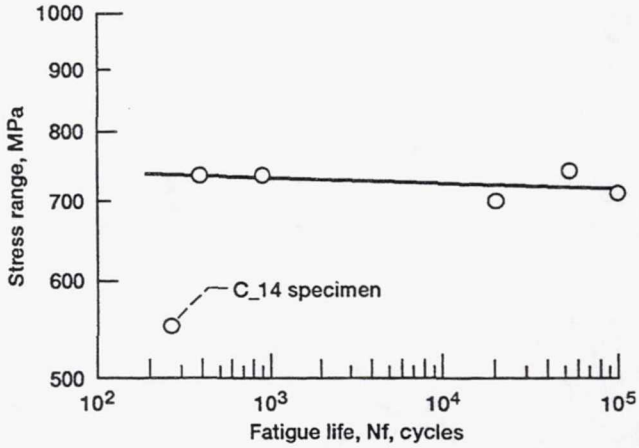

Figure 8.—Fatigue life-stress range curve for C+E material tested at 300 K.

Figure 9.—Fractograph showing large teardrop shaped void (arrow) at crack initiation site in C+E specimen tested at 300 K ($\Delta\epsilon_p \approx 0.10$ percent; $N_f = 269$).

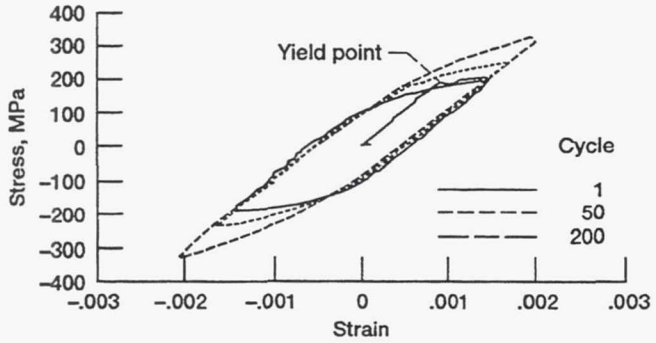

Figure 10.—Hysteresis loops for C+E NiAl tested at 300 K ($\Delta\epsilon_p$ = 0.10 percent; N_f = 929).

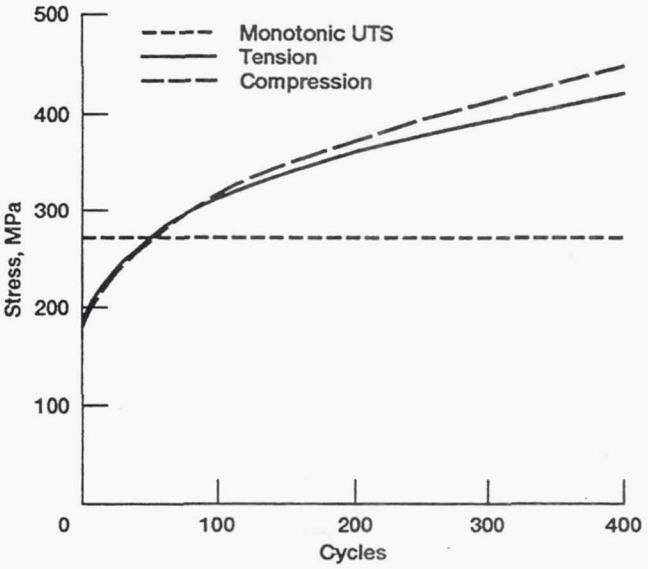

Figure 11.—Response stress (absolute values of stress amplitude) plot for C+E NiAl tested at 300 K ($\Delta\epsilon_p$ = 0.20 percent; N_f = 407).

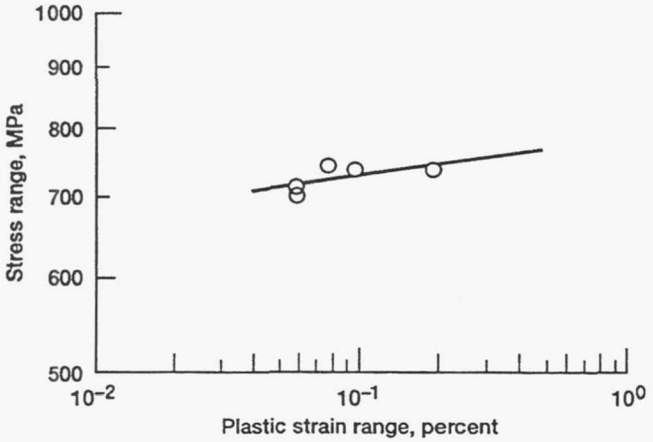

Figure 12.—Cyclic stress-strain curve for C+E NiAl tested at 300 K.

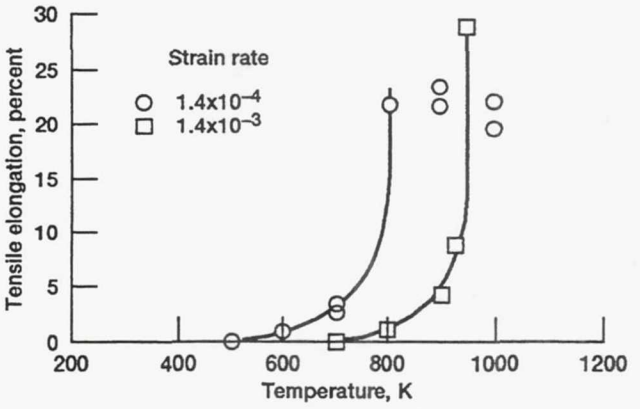

Figure 13.—Tensile ductility as a function of temperature and strain rate for HP NiAl.

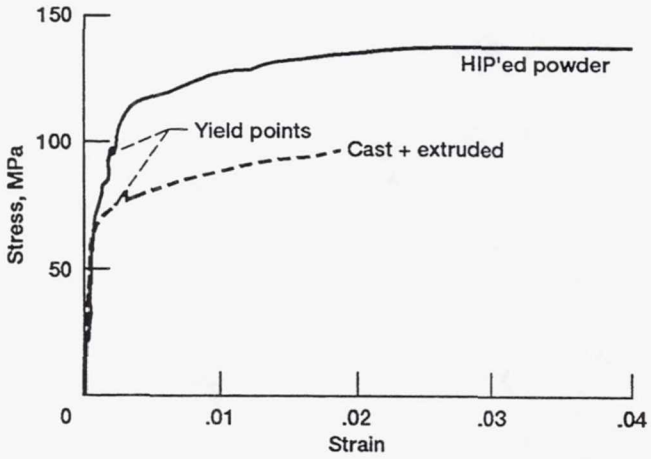

Figure 14.—A portion of tensile curves for C+E and HP NiAl tested at 1000 K.

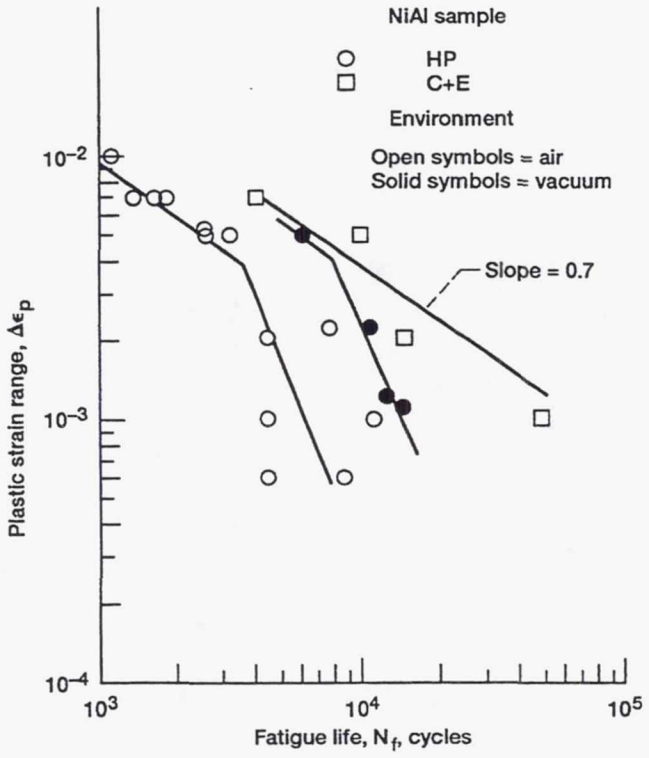

Figure 15.—Fatigue life-plastic strain range curves for C+E and HP NiAl tested at 1000 K.

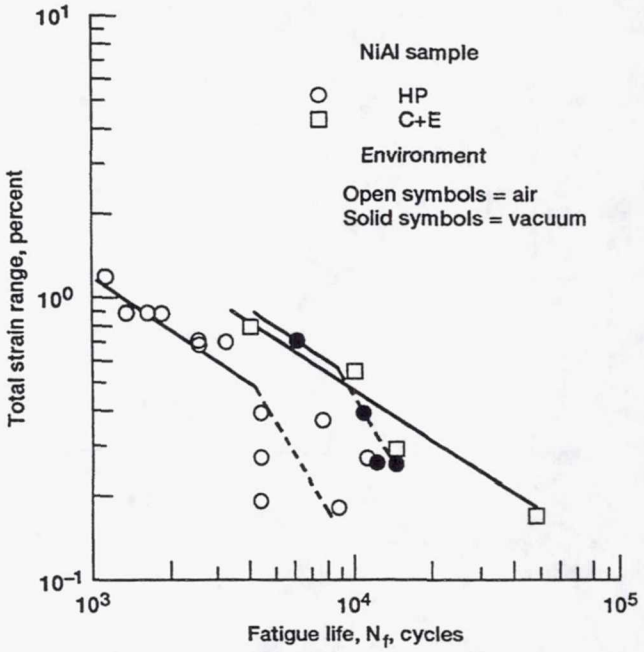

Figure 16.—Fatigue life-total strain range curves for C+E and HP NiAl tested at 1000 K.

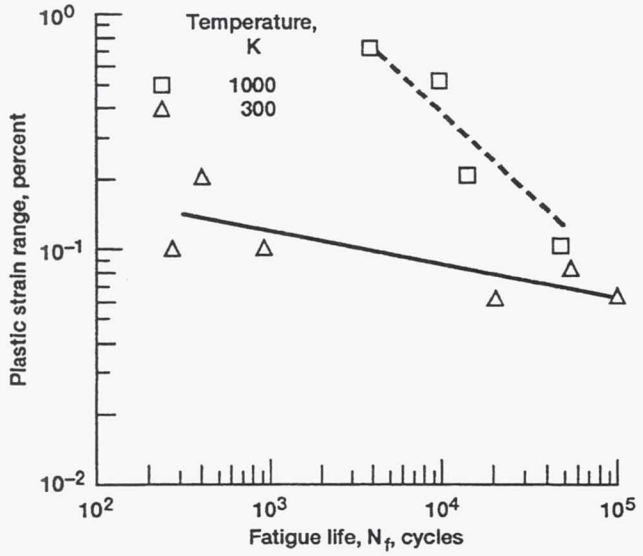

Figure 17.—Comparison of C+E NiAl fatigue life curves at 300 and 1000 K.

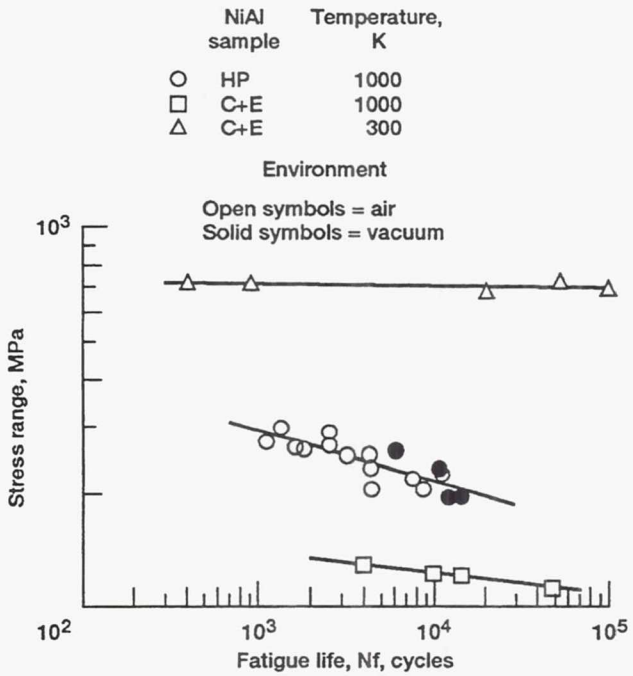

Figure 18.—Fatigue life-stress range curves for C+E and HP NiAl in various environments.

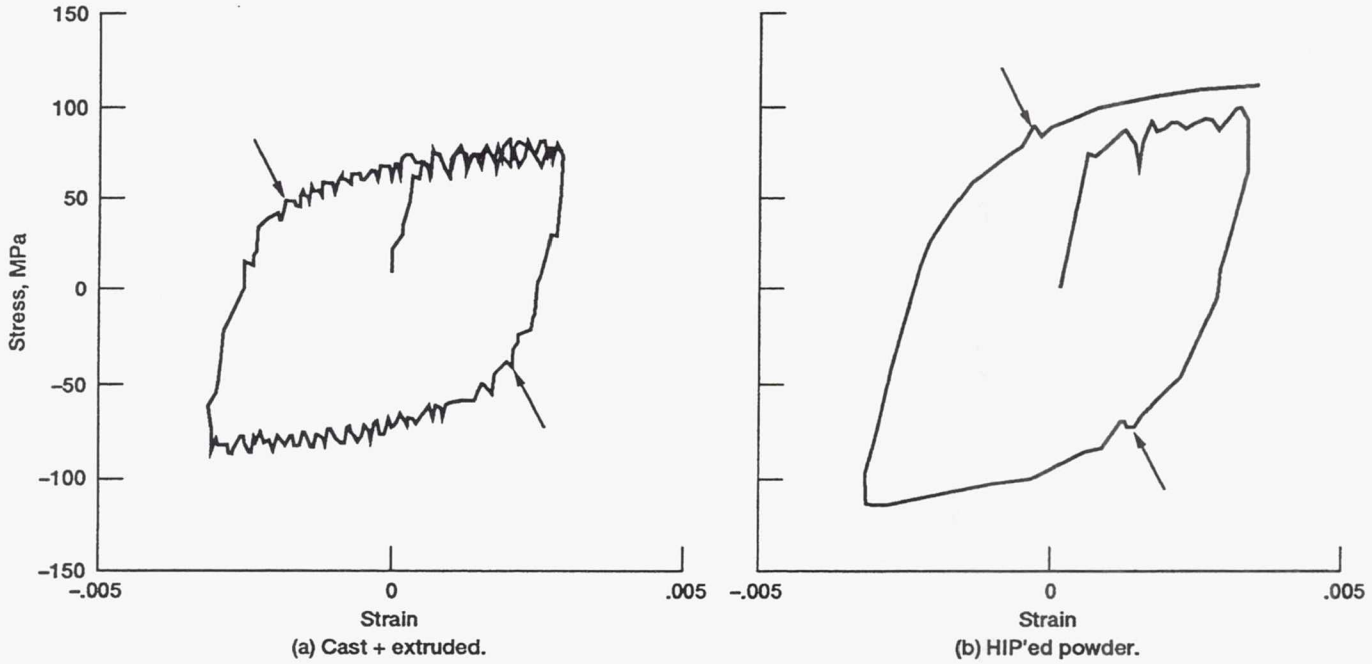

Figure 19.—Hysteresis loops for first cycle of C+E and HP specimens tested at 1000 K (arrows indicate yield points; $\Delta\epsilon_p$ = 0.50 percent).

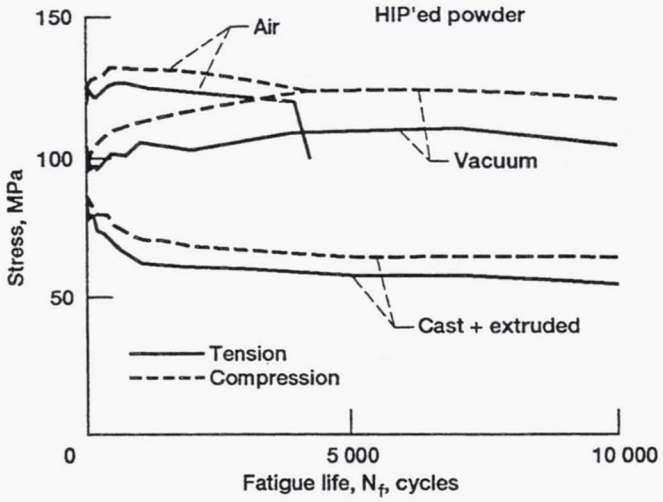

Figure 20.—Response stress (absolute values of stress amplitude) plots for C+E and HP specimens tested at 1000 K ($\Delta\epsilon_p$ = 0.20 percent).

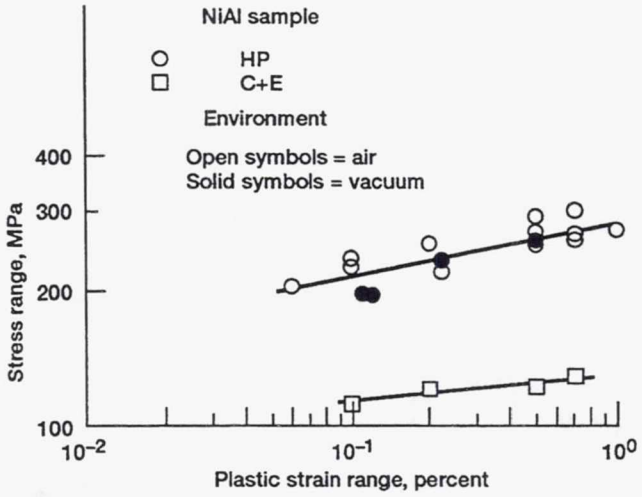

Figure 21.—Cyclic stress-plastic strain curves for C+E and HP specimens tested at 1000 K.

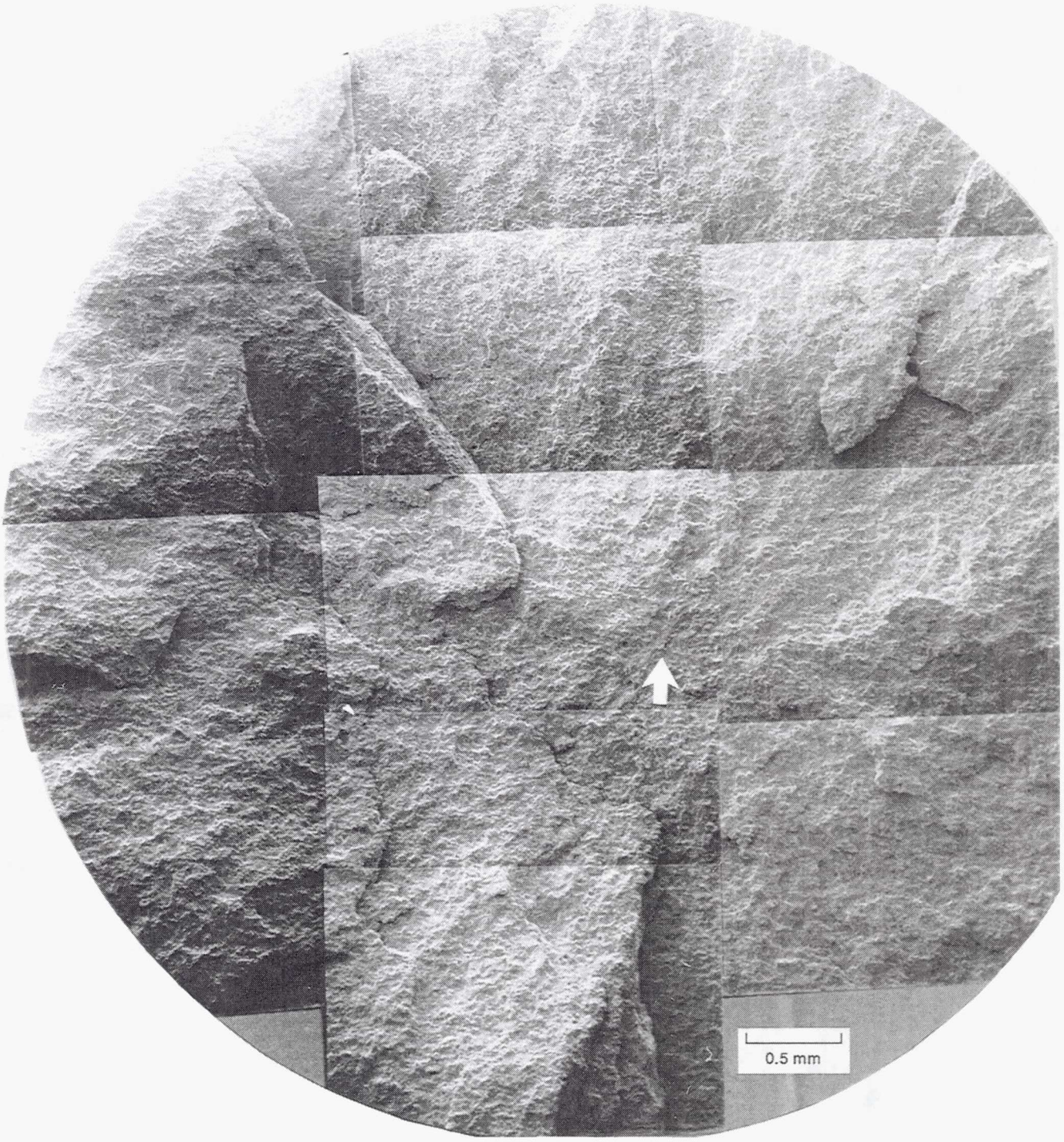

Figure 22.—SEM fractograph of fracture surface in HP specimen tested at 300 K (arrow indicates initiation site; $\Delta\epsilon_p$ = 0.10 percent; N_f = 929).

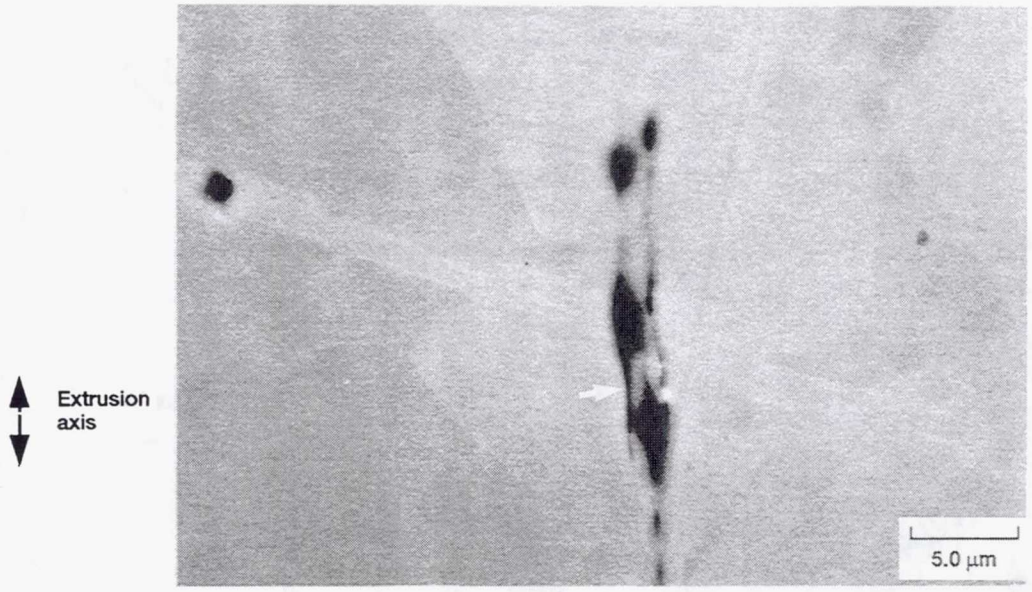

Figure 23.—SEM micrograph of as-extruded NiAl material (arrow indicates processing defect).

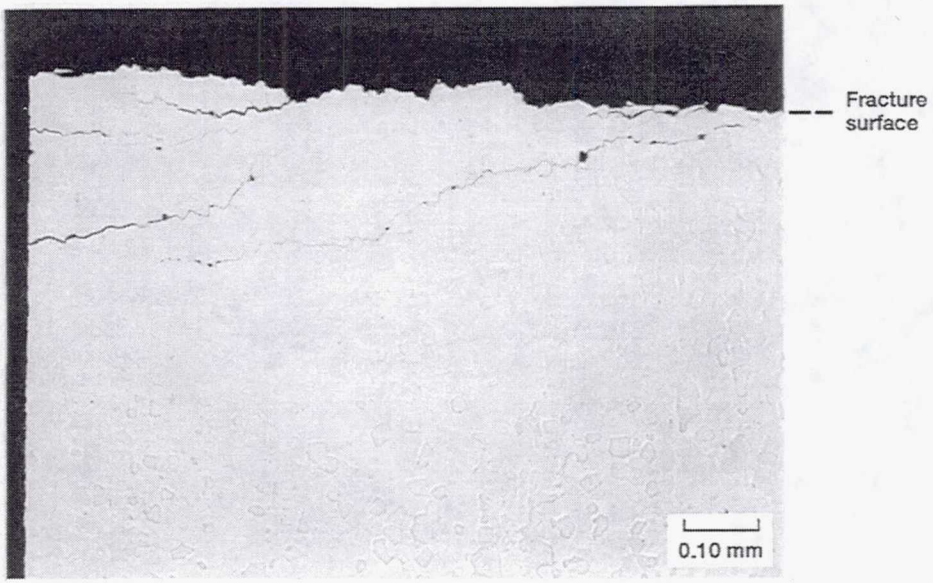

Figure 24.—Optical micrograph of fracture surface of C+E specimen tested at 300 K ($\Delta\epsilon_p$ = 0.20 percent; N_f = 407).

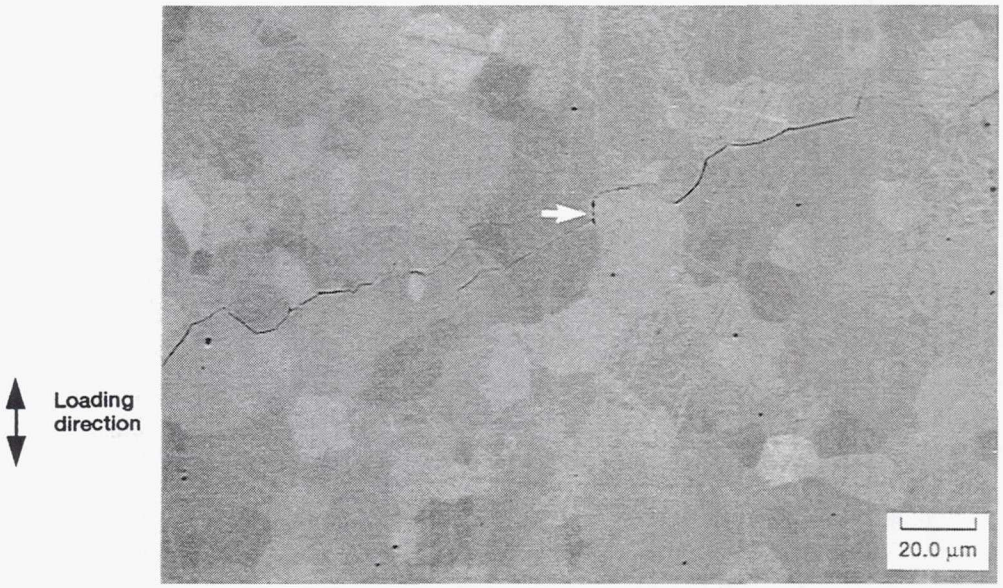

Figure 25.—Backscattered SEM photomicrograph of C+E material illustrating intergranular cracking and interaction with a stringer (arrow) in a specimen tested at 300 K ($\Delta\epsilon_p$ = 0.20 percent; N_f = 407).

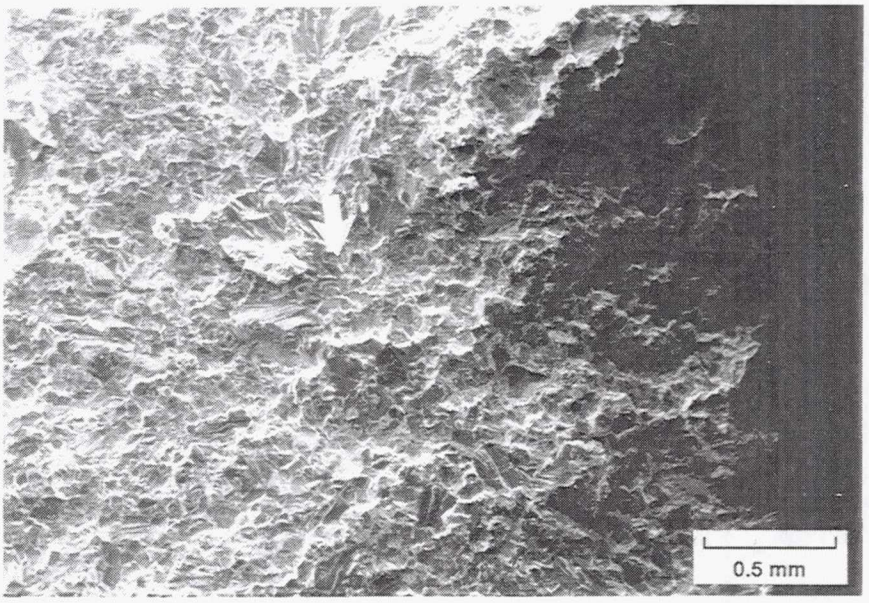

Figure 26.—SEM fractograph showing initiation site (arrow) in HP NiAl specimen tested at 1000 K ($\Delta\epsilon_p$ = 0.70 percent; N_f = 1828).

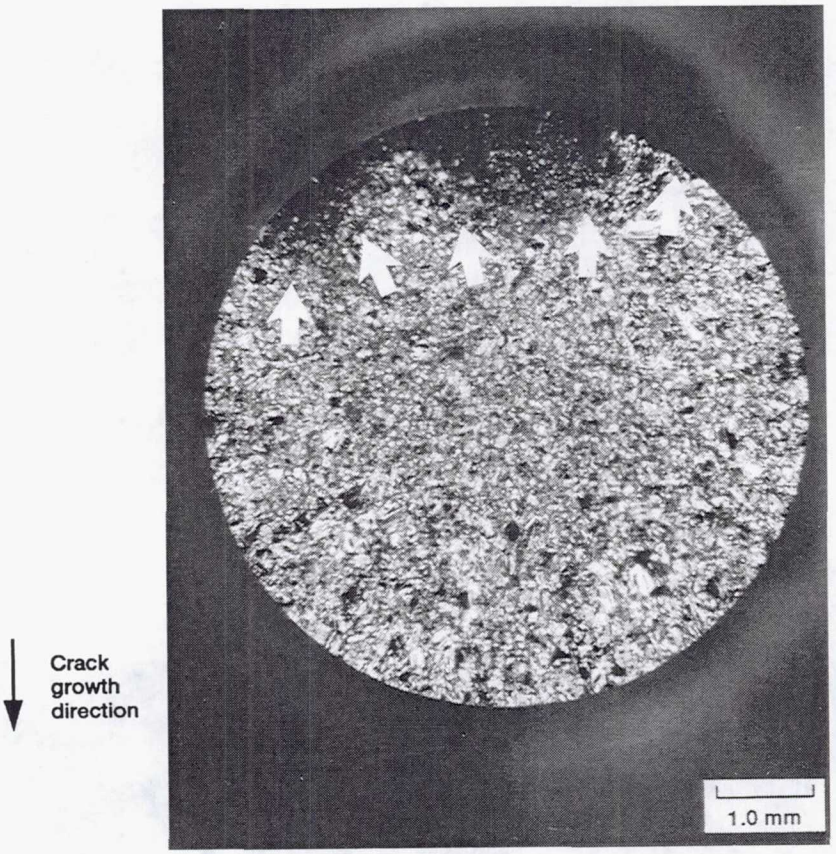

(a) Optical fractograph.

Figure 27.—Fracture surface of HP sample tested at 1000 K. Arrows indicate extent of slow crack growth ($\Delta\epsilon_p$ = 0.70 percent; N_f = 1828).

(b) SEM fractograph.

Figure 27.— Concluded.

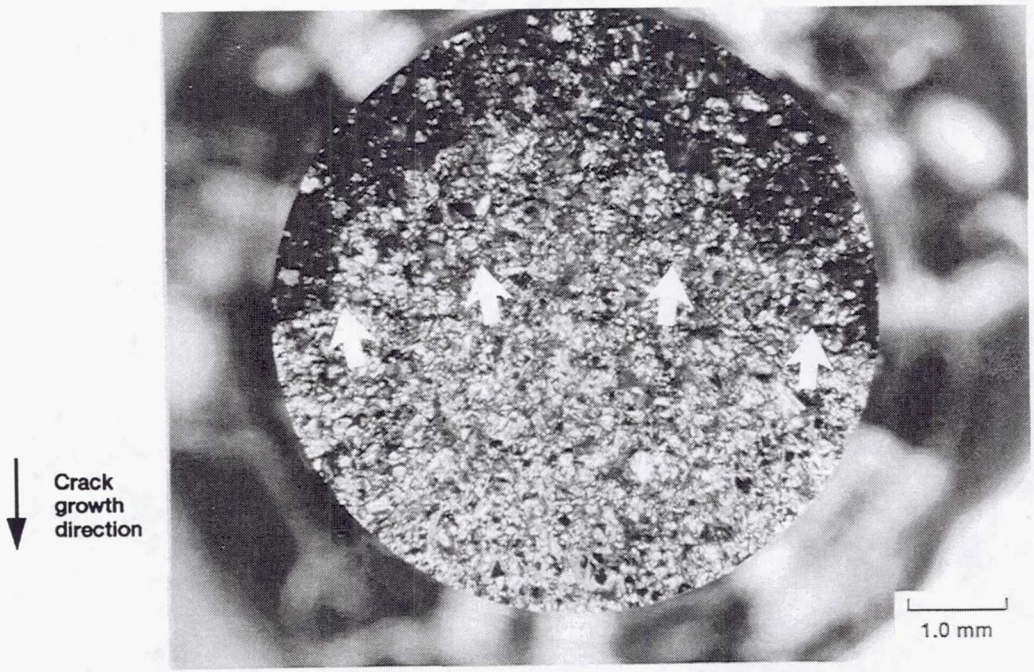

(a) Optical fractograph.

Figure 28.—Fracture surfaces indicating the extent of slow crack growth (arrows) for HP specimen tested at 1000 K ($\Delta\epsilon_p$ = 0.06 percent; N_f = 8662).

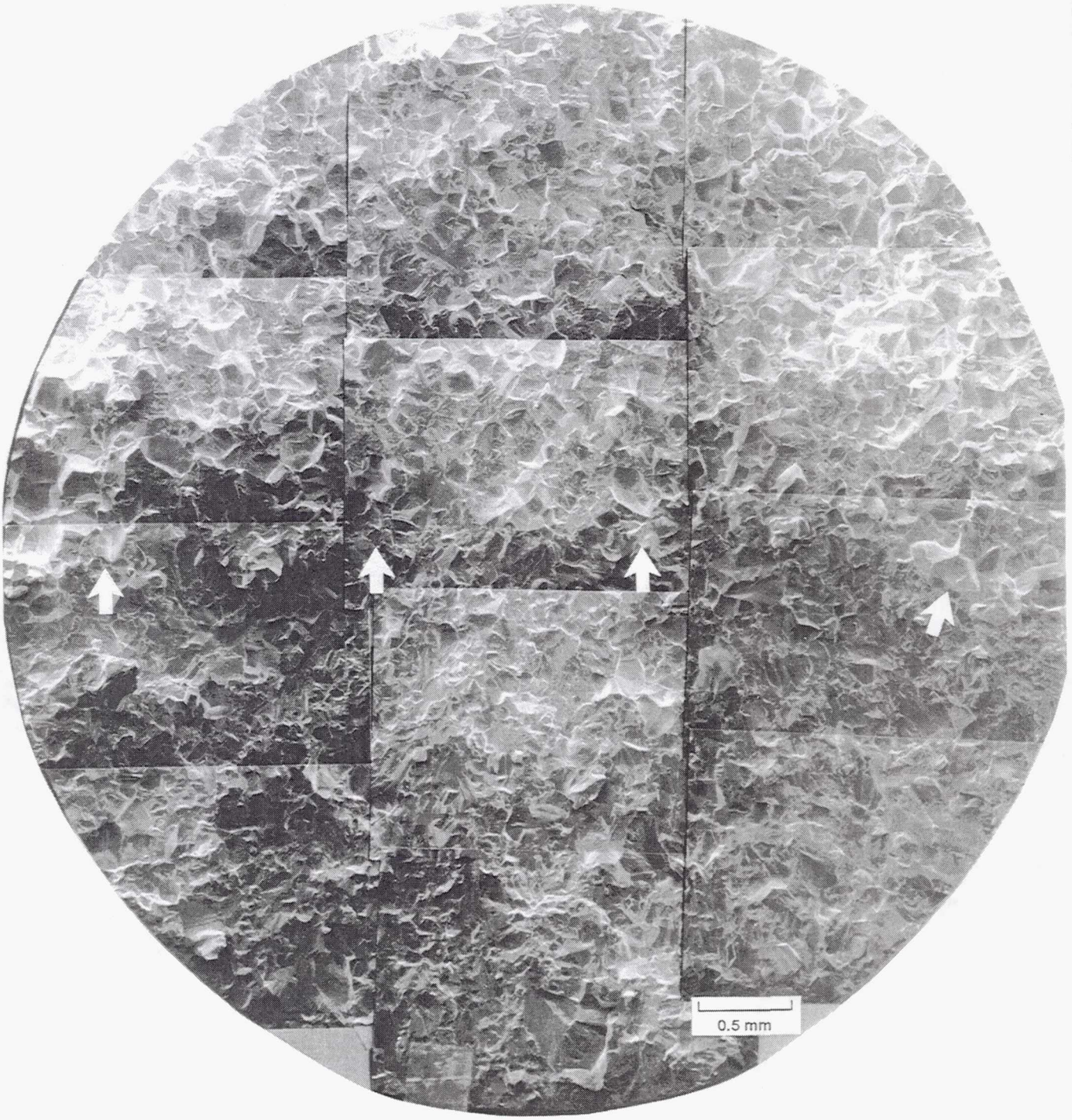

(b) SEM fractograph.

Figure 28.— Concluded.

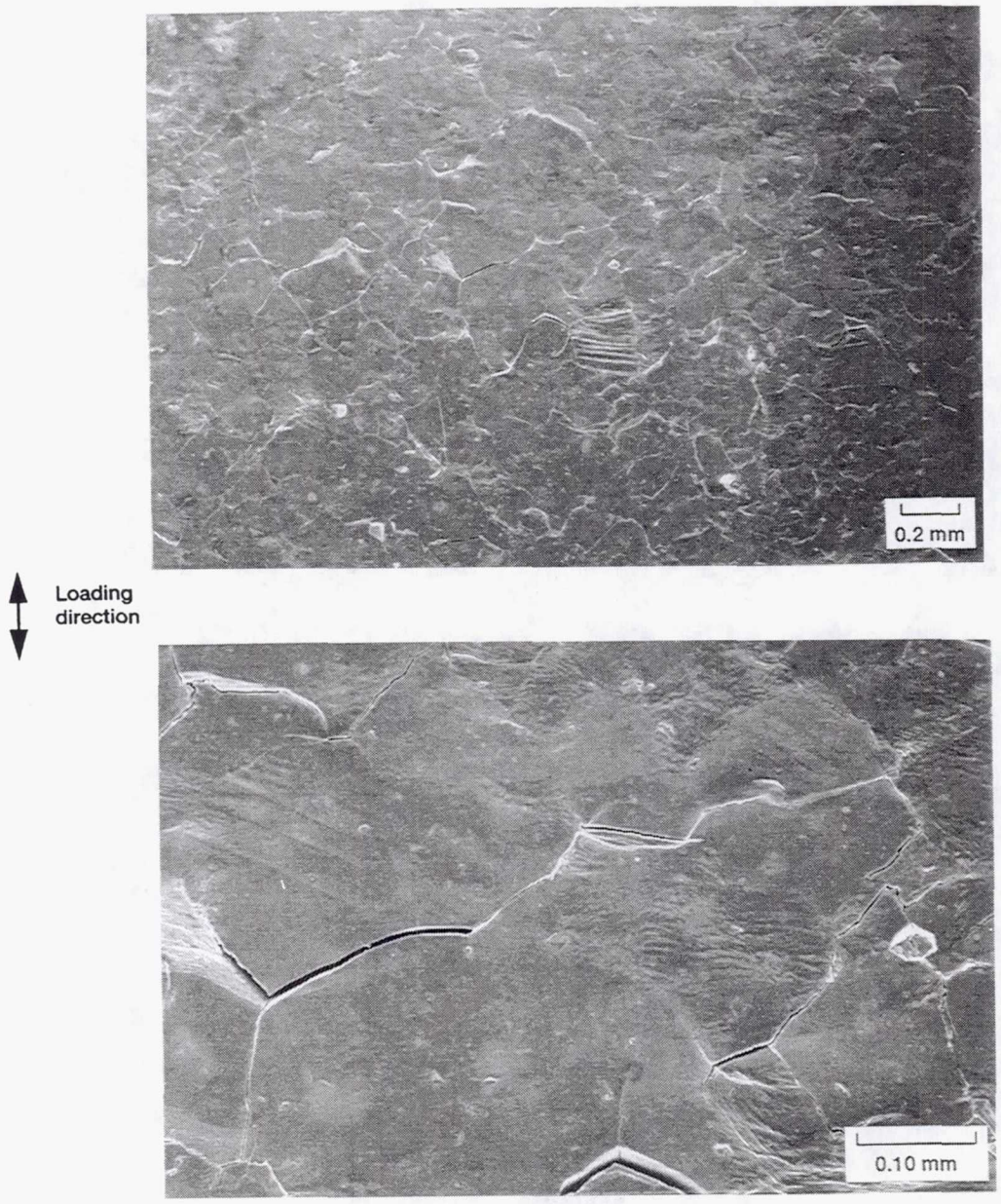

Figure 29.—SEM photomicrographs of intergranular cracks and plastically deformed grains on gauge surface of HP specimen tested at 1000 K ($\Delta\epsilon_p$ = 0.70 percent; N_f = 1828).

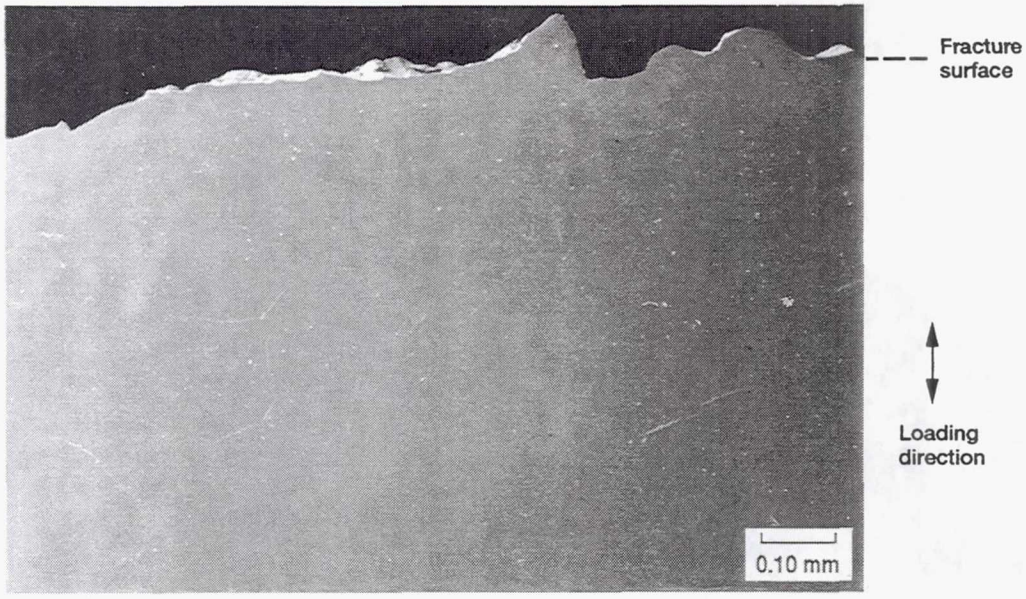

Figure 30.—SEM photomicrograph of limited gauge surface damage for HP specimen tested at 1000 K ($\Delta\epsilon_p$ = 0.06 percent; N_f = 8662).

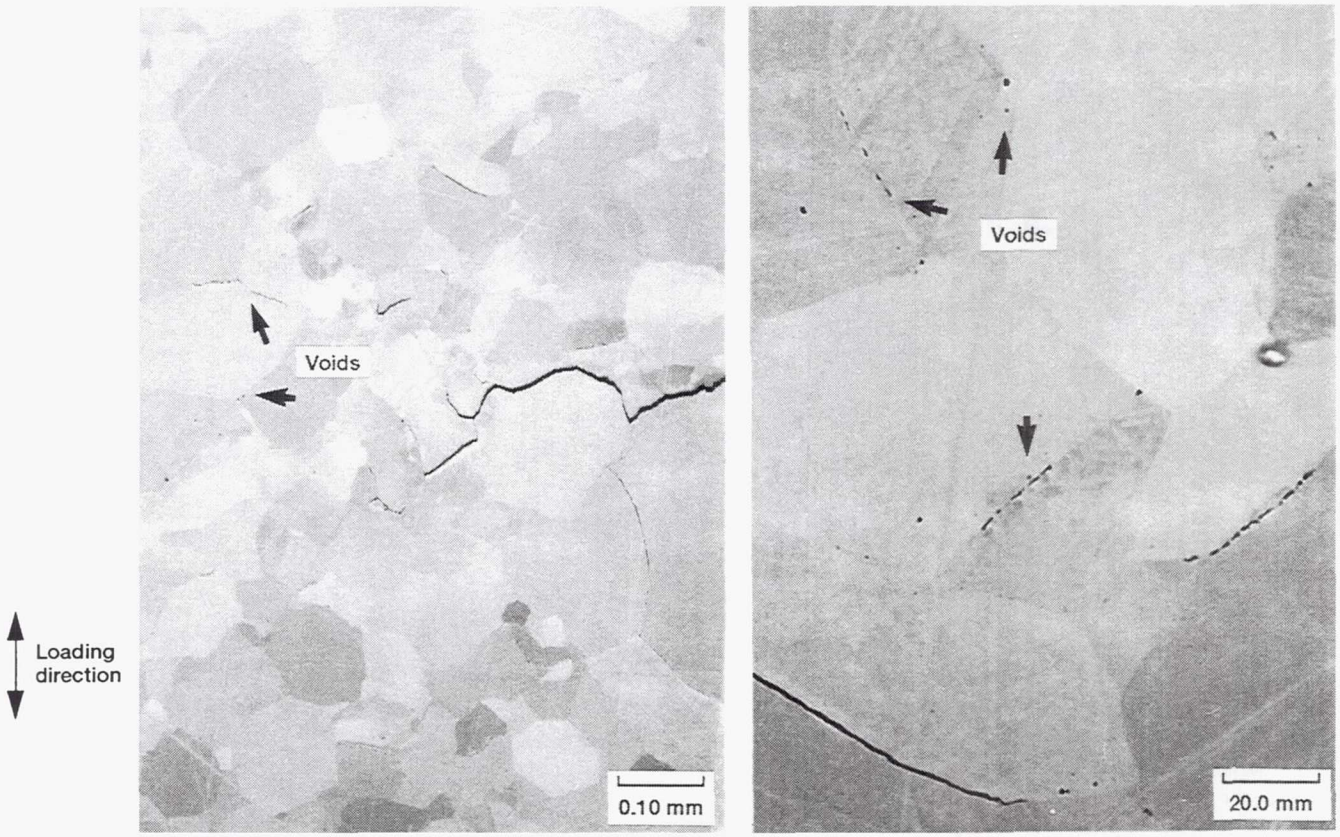

Figure 31.—Backscattered SEM micrographs of surface crack for HP specimen tested at 1000 K ($\Delta\epsilon_p$ = 0.10 percent; N_f = 11 088). Arrows indicate grain boundary voids.

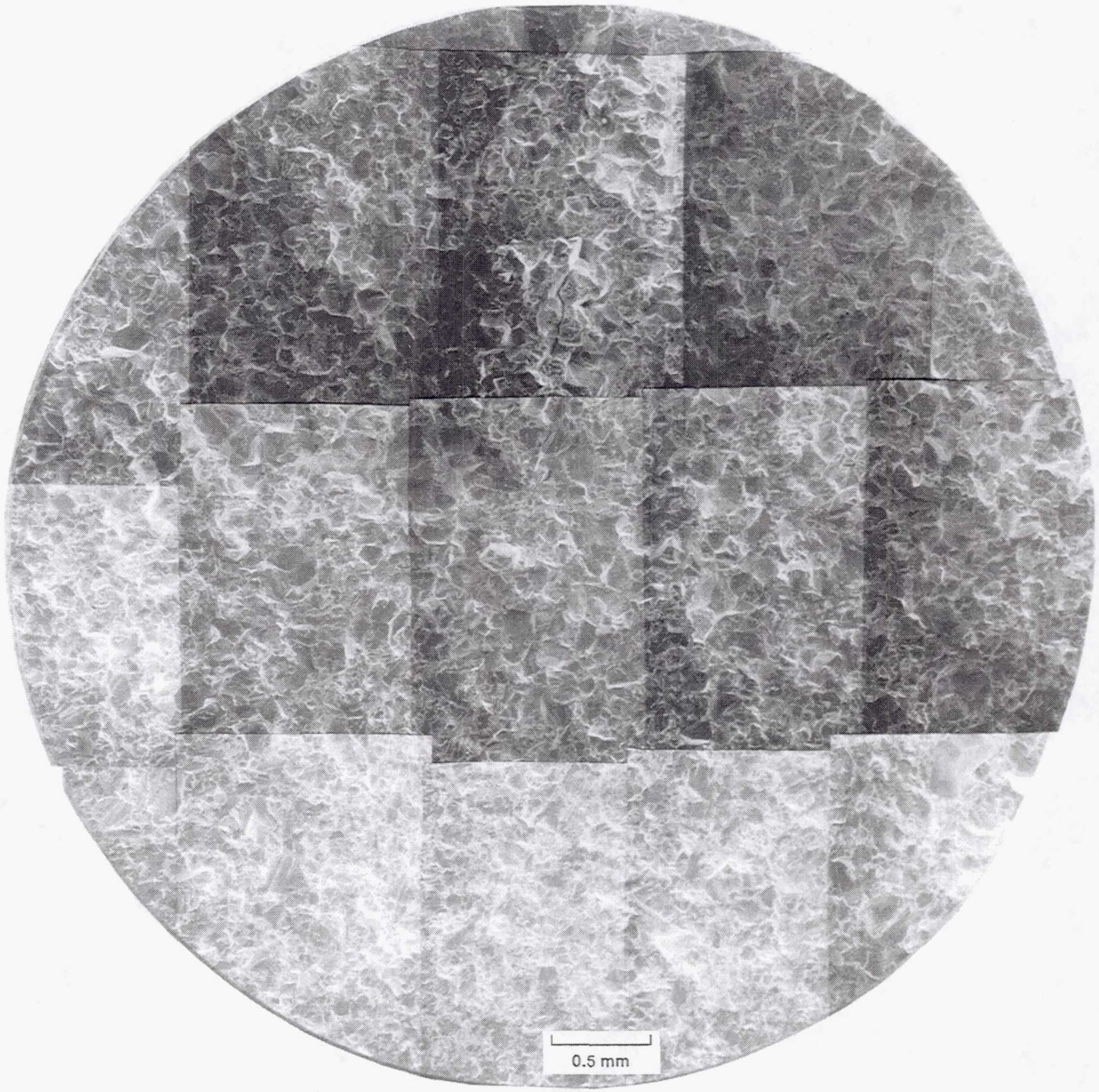

Figure 32.— SEM fractograph of HP specimen tested at 1000 K in vacuum ($\Delta\epsilon_p$ = 0.11 percent; N_f = 14 327).

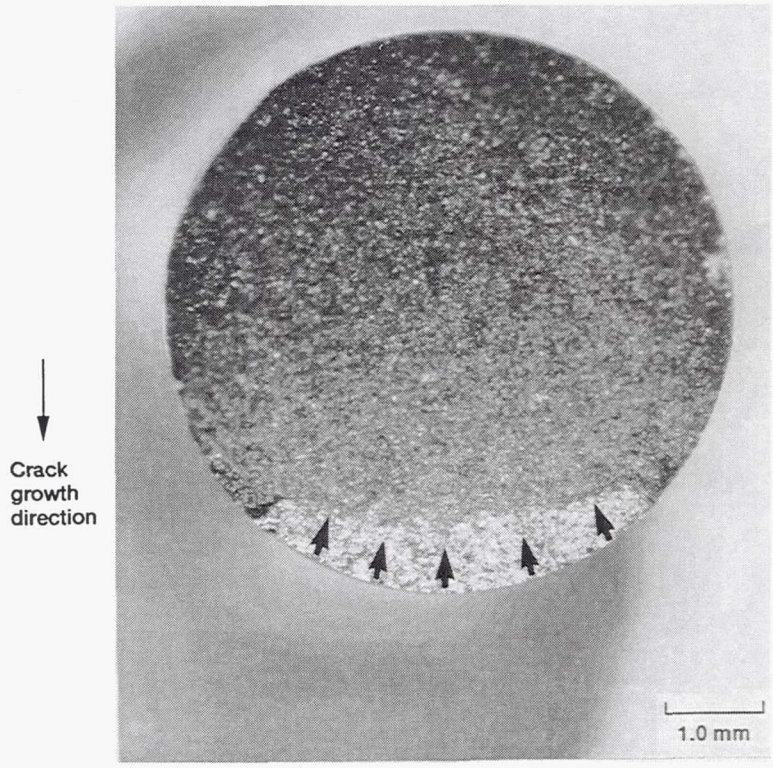

(a) Optical fractograph.

Figure 33.—Fractographs indicating the extent of slow fatigue crack growth at low plastic strain range (arrows) in C+E specimen tested at 1000 K ($\Delta\epsilon_p$ = 0.10 percent; N_f = 48 090).

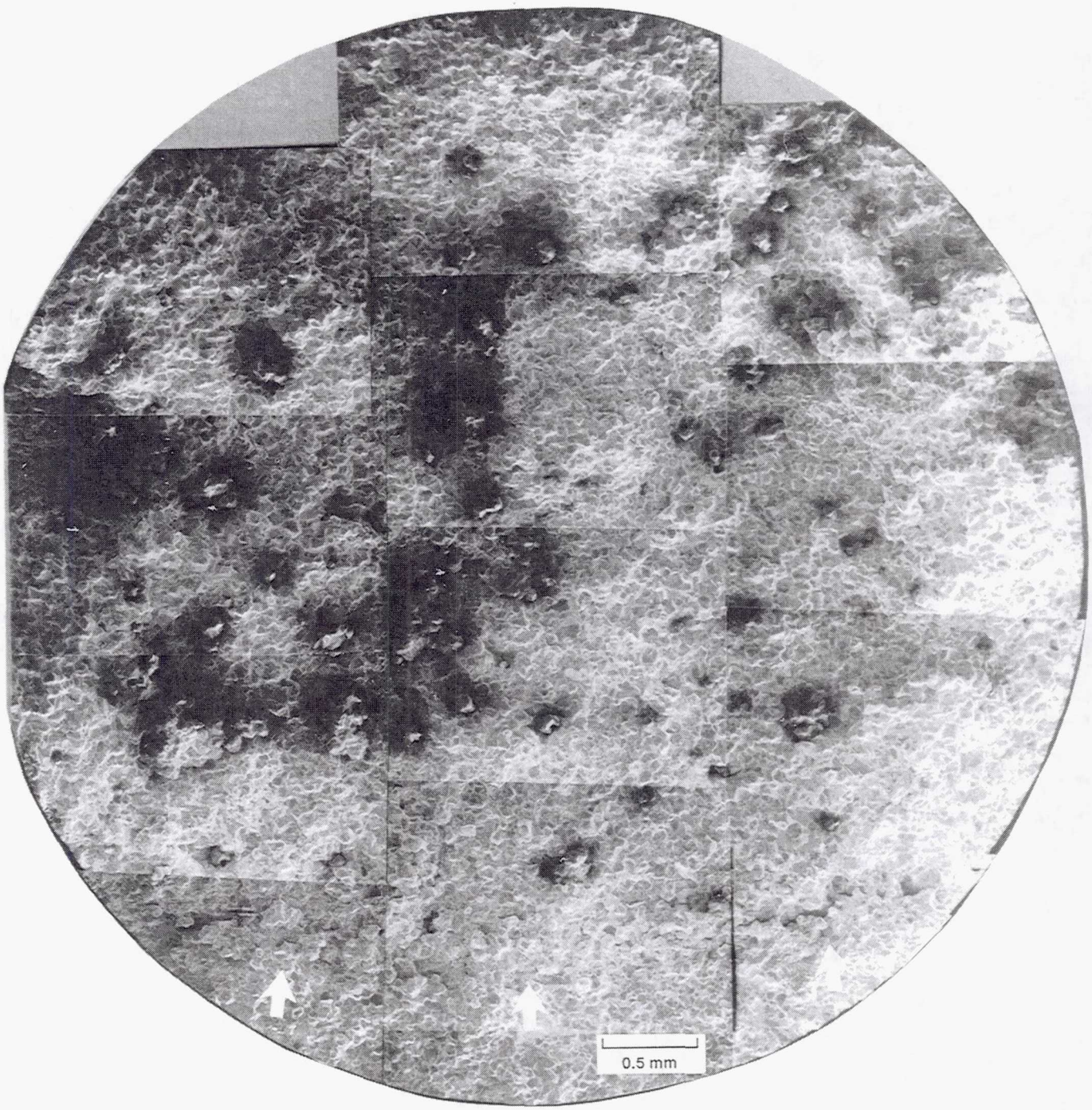

(b) SEM fractograph.

Figure 33.— Concluded.

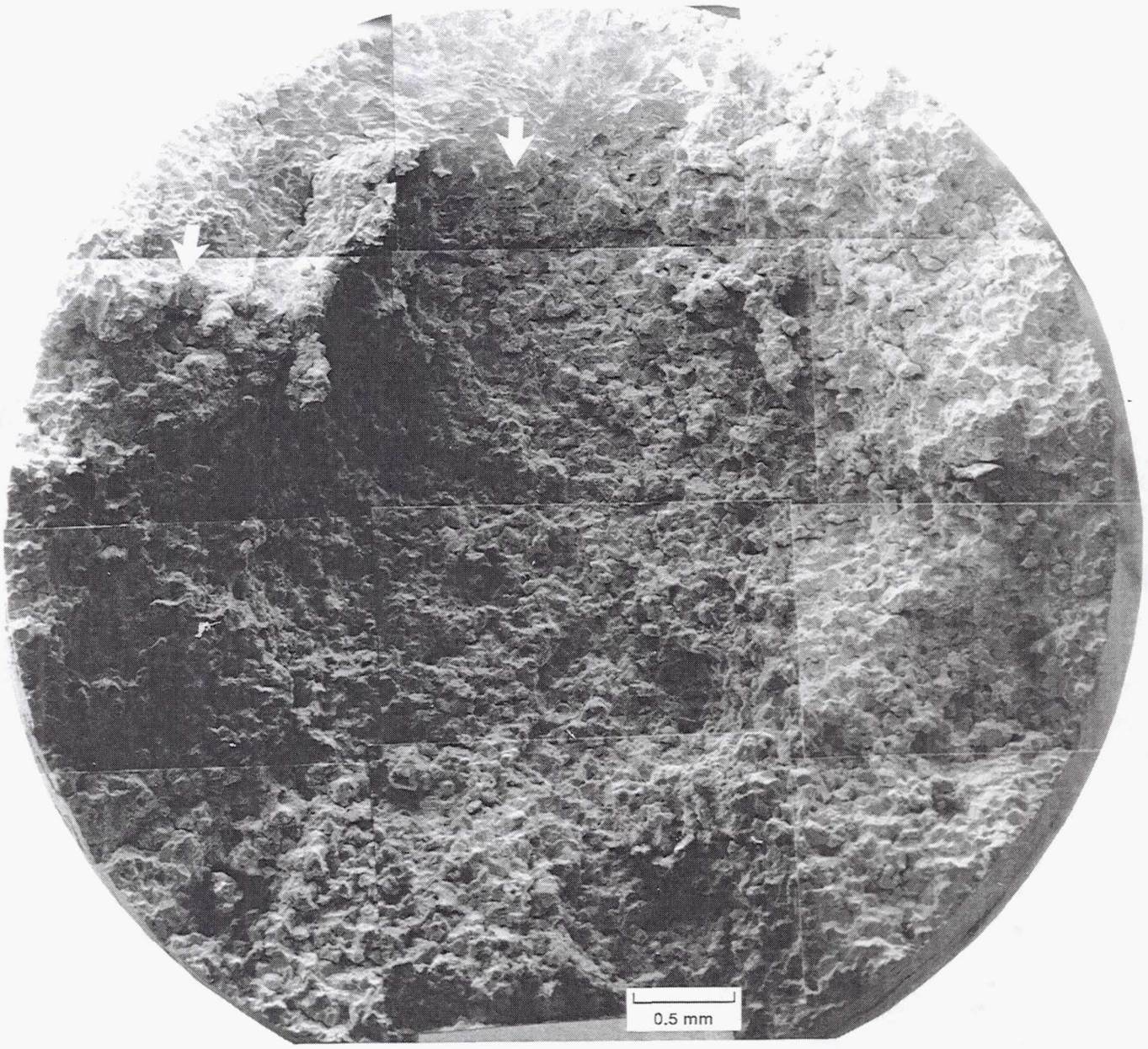

Figure 34.— Fractograph indicating the extent of slow fatigue crack growth at high plastic strain range (arrows) in C+E NiAl specimen tested at 1000 K ($\Delta\epsilon_p$ = 0.50 percent; N_f = 9918).

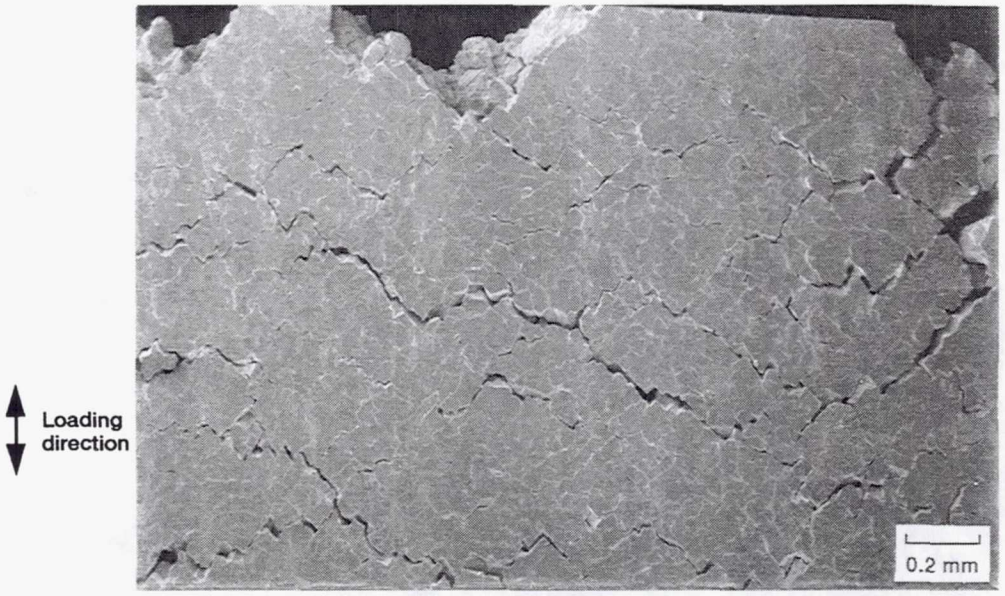

Figure 35.—SEM photomicrograph of the gauge surface of C+E NiAl specimen tested at 1000 K showing intergranular cracking ($\Delta\epsilon_p$ = 0.50 percent; N_f = 9918).

Figure 36.—SEM photomicrograph of the gauge surface of C+E NiAl specimen tested at 1000 K illustrating very limited damage ($\Delta\epsilon_p$ = 0.10 percent; N_f = 48 090).

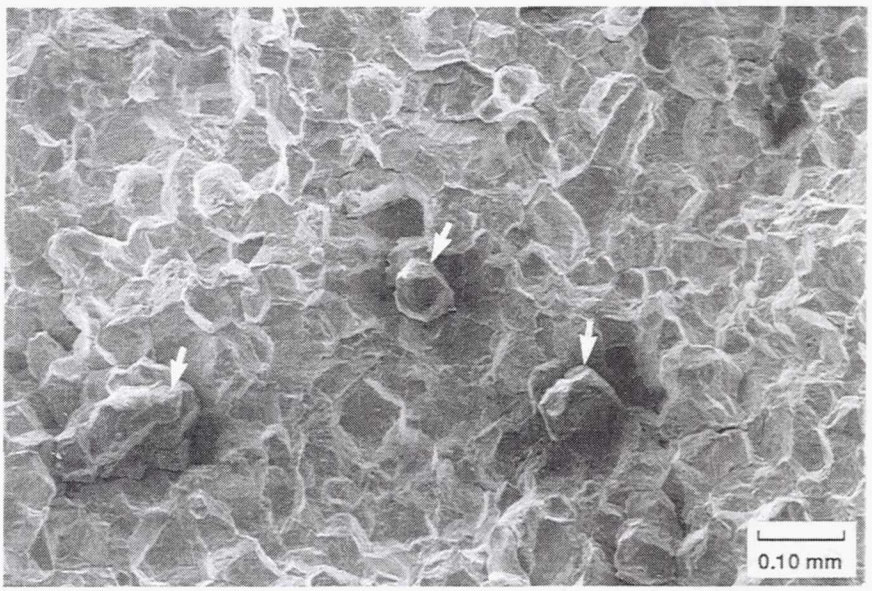

Figure 37.—SEM photomicrograph showing a number of grains (arrows) that were almost completely torn free from the sample surface ($\Delta\epsilon_p$ = 0.10 percent; N_f = 48 090).

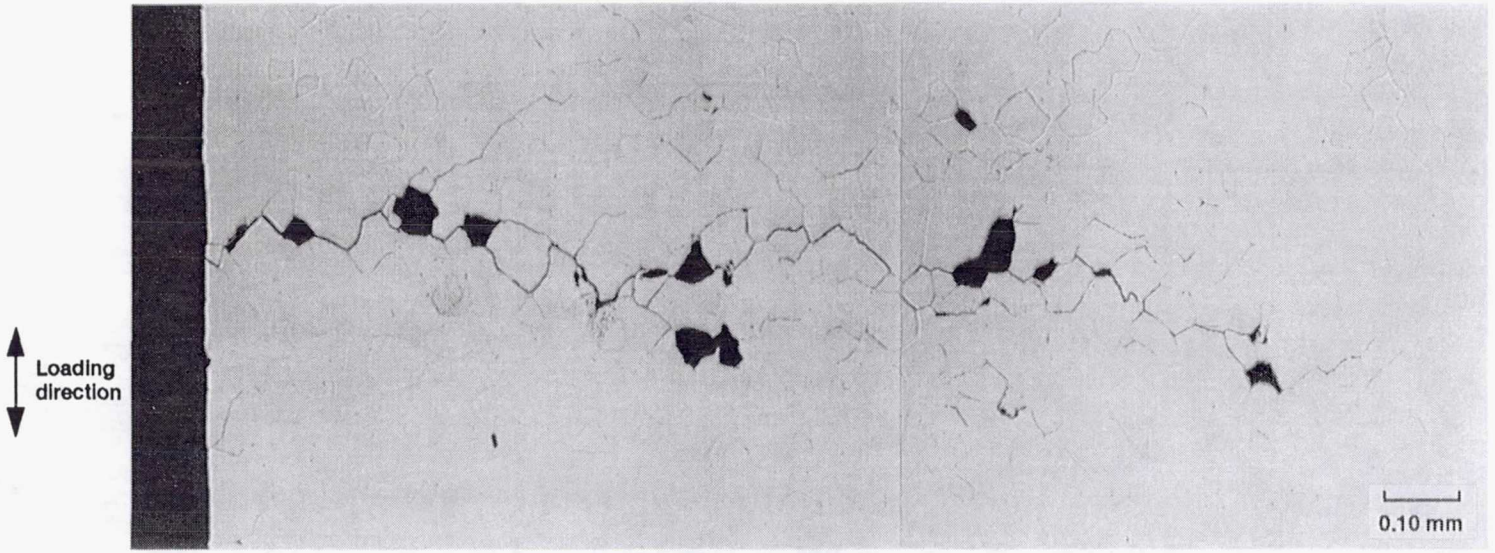

Figure 38.—Optical micrograph of intergranular cracking in C+E NiAl specimen tested at 1000 K. Arrows indicate missing grains that were damaged during fatigue and pulled-out during metallographic preparation ($\Delta\epsilon_p$ = 0.10 percent; N_f = 48 090).

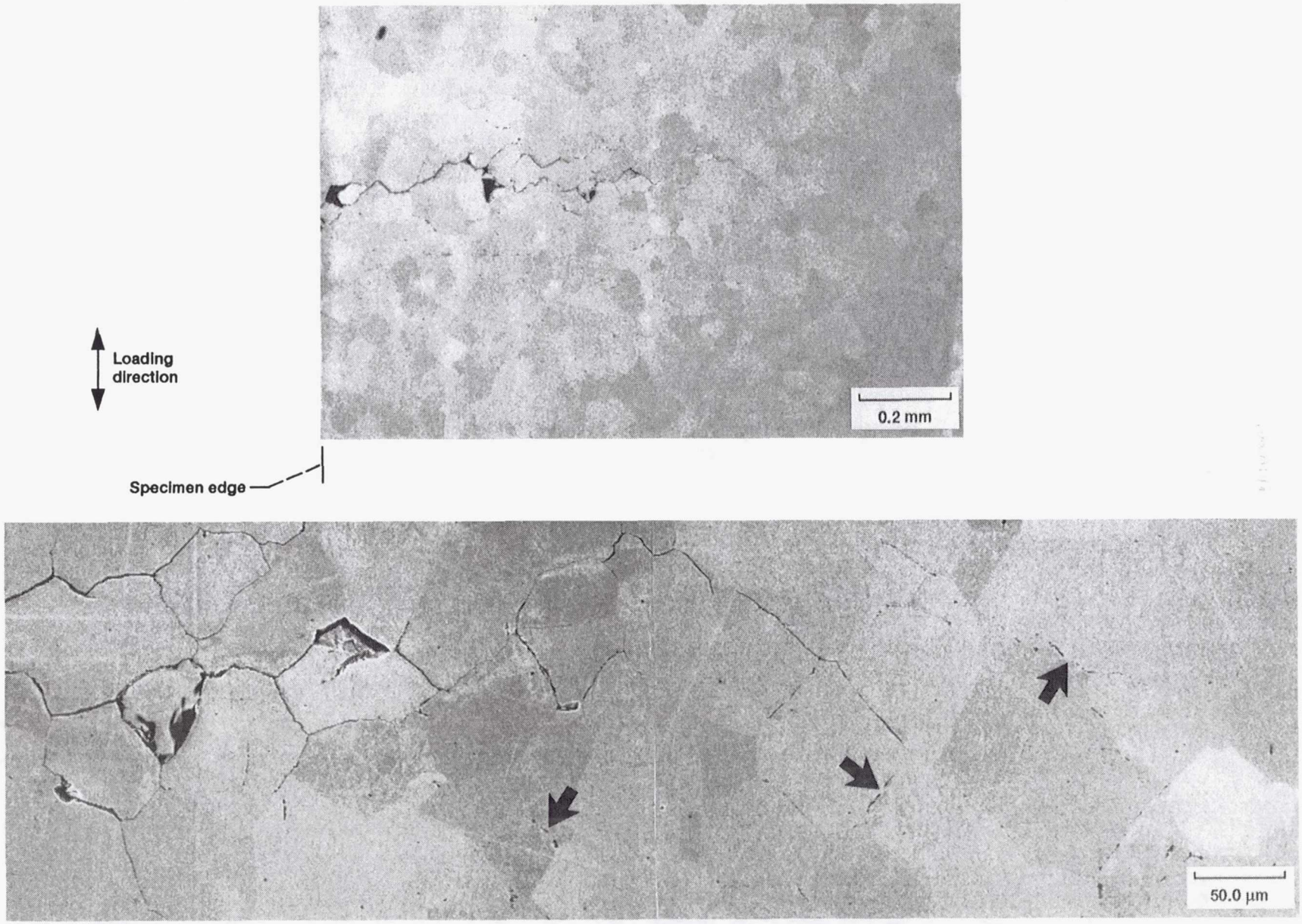

Figure 39.—Backscattered SEM photomicrograph of intergranular cracking in C+E NiAl specimen tested at 1000 K ($\Delta\epsilon_p$ = 0.10 percent; N_f = 48 090). Arrows indicate grain boundary pores.

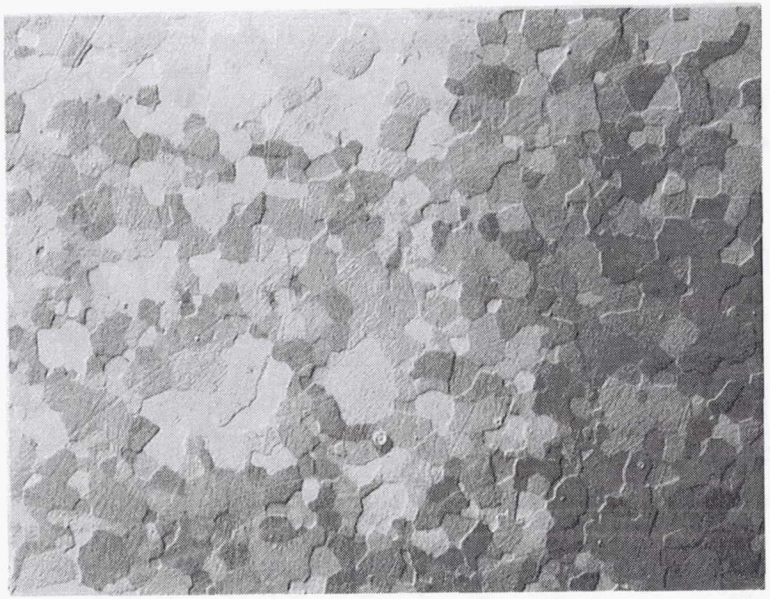

(a) As-received grain size is 18 μm.

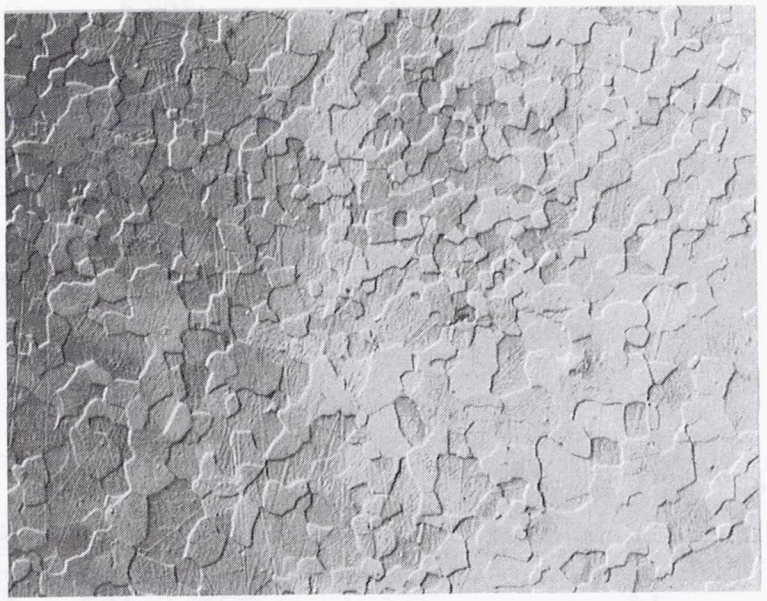

(b) Grain size is 18 μm after 80 h at 1000 K.

50.0 μm

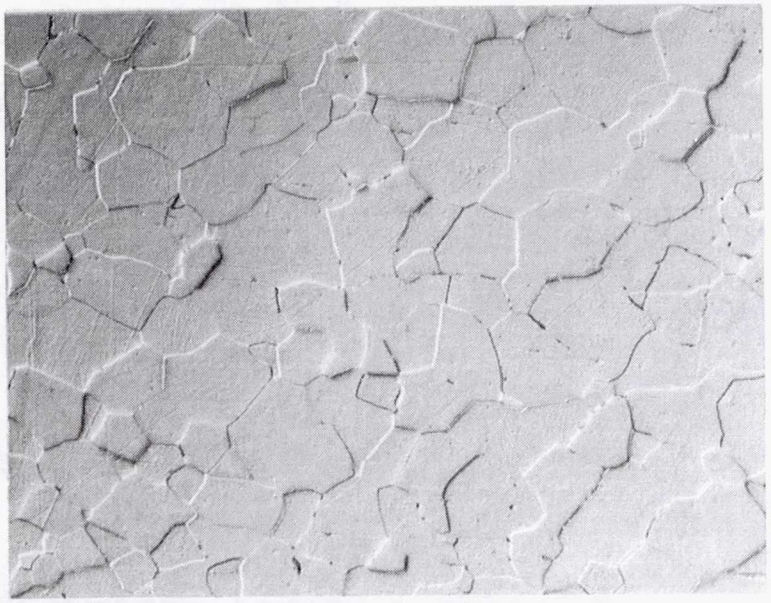

(c) Grain size is 75 μm after fatigue testing at 1000 K.

Figure 40.—Typical microstructure for C+E NiAl specimens. Etchant: Kalling's. Differential interference contrast illumination.

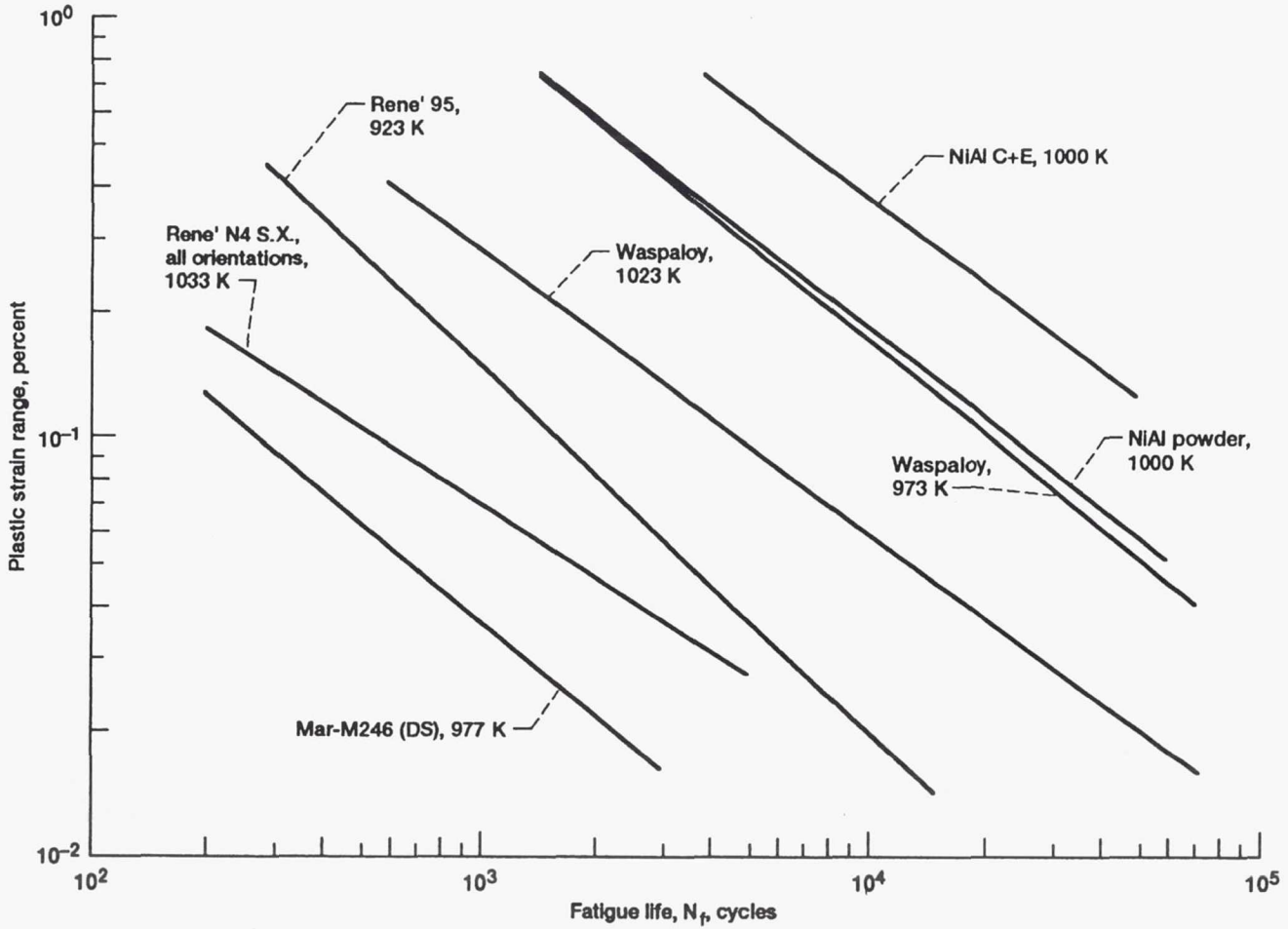

Figure 41.—Fatigue life of NiAl compared to Ni-base superalloys on plastic strain range basis at nominally 1000 K.

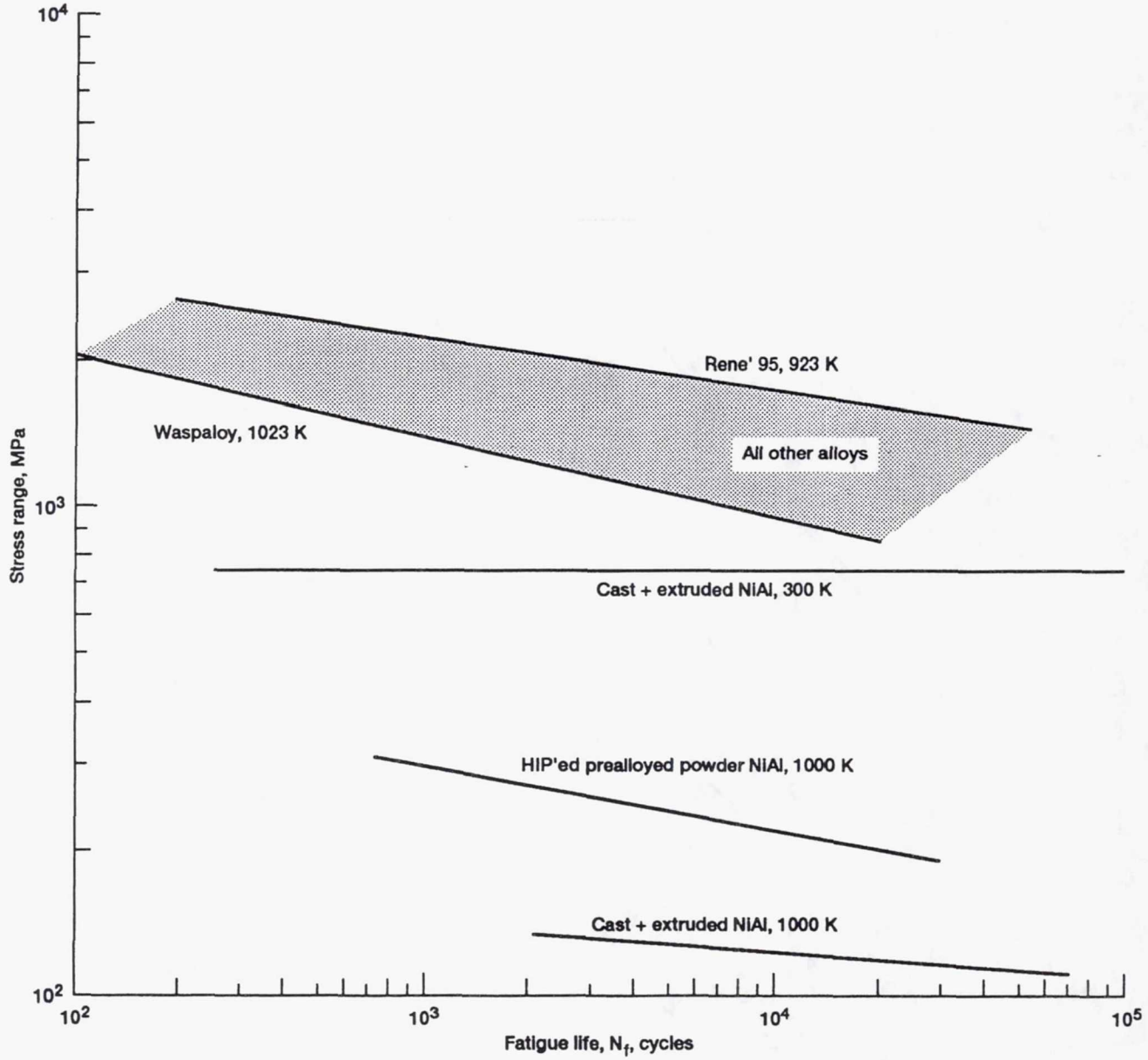

Figure 42.—Fatigue life of NiAl compared to Ni-base superalloys on a stress range basis at nominally 1000 K.

REPORT DOCUMENTATION PAGE

Form Approved
OMB No. 0704-0188

1. AGENCY USE ONLY (*Leave blank*)	2. REPORT DATE	3. REPORT TYPE AND DATES COVERED
	April 1993	Technical Memorandum

4. TITLE AND SUBTITLE

Low Cycle Fatigue Behavior of Polycrystalline NiAl at 300 and 1000 K

5. FUNDING NUMBERS

WU-510-01-50

6. AUTHOR(S)

Bradley A. Lerch and Ronald D. Noebe

7. PERFORMING ORGANIZATION NAME(S) AND ADDRESS(ES)

National Aeronautics and Space Administration
Lewis Research Center
Cleveland, Ohio 44135-3191

8. PERFORMING ORGANIZATION REPORT NUMBER

E-7566

9. SPONSORING/MONITORING AGENCY NAMES(S) AND ADDRESS(ES)

National Aeronautics and Space Administration
Washington, D.C. 20546-0001

10. SPONSORING/MONITORING AGENCY REPORT NUMBER

NASA TM-105987

11. SUPPLEMENTARY NOTES

Responsible person, Bradley A. Lerch, (216) 433-5522.

12a. DISTRIBUTION/AVAILABILITY STATEMENT

Unclassified - Unlimited
Subject Category 26

12b. DISTRIBUTION CODE

13. ABSTRACT ***(Maximum 200 words)***

The low cycle fatigue behavior of polycrystalline NiAl was determined at 300 and 1000 K—temperatures below and above the brittle-to-ductile transition temperature (BDTT). Fully reversed, plastic strain-controlled fatigue tests were conducted on two differently fabricated alloy samples: hot isostatically pressed (HIP'ed) prealloyed powder and hot extruded castings. HIP'ed powder (HP) samples were tested only at 1000 K, whereas the more ductile cast-and-extruded (C+E) NiAl samples were tested at both 1000 and 300 K. Plastic strain ranges of 0.06 to 0.2 percent were used. The C+E NiAl cyclically hardened until fracture, reaching stress levels approximately 60 percent greater than the ultimate tensile strength of the alloy. Compared on a strain basis, NiAl had a much longer fatigue life than other B2 ordered compounds in which fracture initiated at processing-related defects. These defects controlled fatigue life at 300 K, with fracture occurring rapidly once a critical stress level was reached. At 1000 K, above the BDTT, both the C+E and HP samples cyclically softened during most of the fatigue tests in air and were insensitive to processing defects. The processing method did not have a major effect on fatigue life; the lives of the HP samples were about a factor of three shorter than the C+E NiAl, but this was attributed to the lower stress response of the C+E material. The C+E NiAl underwent dynamic grain growth, whereas the HP material maintained a constant grain size during testing. In both materials, fatigue life was controlled by intergranular cavitation and creep processes, which led to fatigue crack growth that was primarily intergranular in nature. Final fracture by overload was transgranular in nature. Also, HP samples tested in vacuum had a life three times longer than their counterparts tested in air and, in contrast to those tested in air, hardened continuously over half of the sample life, thereby indicating an environmentally assisted fatigue damage mechanism. The C+E samples were tested only in air. At 1000 K, NiAl exhibited a superior fatigue life when compared to most superalloys on a plastic strain basis, but was inferior to most superalloys on a stress basis.

14. SUBJECT TERMS	15. NUMBER OF PAGES
Fatigue; NiAl; Damage mechanisms; Deformation	48
	16. PRICE CODE: A03

17. SECURITY CLASSIFICATION OF REPORT	18. SECURITY CLASSIFICATION OF THIS PAGE	19. SECURITY CLASSIFICATION OF ABSTRACT	20. LIMITATION OF ABSTRACT
Unclassified	Unclassified	Unclassified	

National Aeronautics and
Space Administration

Lewis Research Center
Cleveland, Ohio 44135